IEEE Access
Multidisciplinary ⋮ Rapid Review ⋮ Open Access Journal

Received 28 November 2023, accepted 22 December 2023, date of publication 29 December 2023,
date of current version 8 January 2024.

Digital Object Identifier 10.1109/ACCESS.2023.3348414

RESEARCH ARTICLE

Low Complexity DOA Estimation of Multiple Coherent Sources Using a Single Direct Data Snapshot

AHMED A. HUSSAIN[1], NIZAR TAYEM[2], (Member, IEEE), AND ABDEL-HAMID SOLIMAN[3]
[1]Department of Electrical Engineering, Prince Mohammad bin Fahd University, Al Khobar 31952, Saudi Arabia
[2]Department of Engineering and Technology, Texas A&M University– Commerce, Commerce, TX 75428, USA
[3]School of Digital, Technologies and Arts, Staffordshire University, ST4 2DE Stoke-on-Trent, U.K.

Corresponding author: Ahmed A. Hussain (ahussain1@pmu.edu.sa)

ABSTRACT The direction of arrival (DOA) estimation of multiple radio frequency (RF) coherent signals using conventional algorithms such as Multiple Signal Classification (MUSIC), Estimation of the Signal Parameters via the Rotational Invariance Technique (ESPRIT), and their variants is computationally complex and usually requires a large number of data snapshots for accurate estimation. As the number of antenna elements grows, particularly in massive MIMO systems, the complexity of real-time DOA estimation algorithms significantly rises, placing higher demands on computational power and memory resources. In this paper, we present an efficient approach that operates effectively with just a single snapshot for DOA estimation of multiple coherent and non-coherent signals. The proposed method has the following advantages over existing methods: 1) constructs a Toeplitz structure data matrix from a single data snapshot; 2) applies forward-backward averaging operation to the data matrix instead of the covariance matrix constructed using hundreds of snapshots; 3) resolves the differences in the noise elements of the data matrix, preserving the conjugate symmetry property of the Toeplitz matrix; 4) converts the complex Toeplitz data matrix to a real-valued matrix in an efficient way without unitary transformations; and 5) employs QR decomposition to extract the signal and noise subspaces, eliminating the need for computationally complex eigenvalue (EVD) or singular value decomposition (SVD). Finally, we establish the effectiveness of our proposed method through both MATLAB simulations and real-time experiments. Compared to existing methods like Unitary root-MUSIC, the proposed approach demonstrates significantly reduced complexity and faster estimation times.

INDEX TERMS Single snapshot, DOA estimation, coherent sources, software defined radio, real-time validation, USRP, Toeplitz matrix, decorrelation, computation time.

I. INTRODUCTION

Estimating the direction of arrival (DOA) angles of RF sources impinging on an array of antennas has emerged as a dynamic field of research with growing significance across diverse practical applications, spanning both civilian and military domains. These applications encompass crucial tasks such as channel equalization and estimation, interference and echo suppression, precise source localization within sonar and radar systems, the deployment of adaptive antenna arrays for intelligent beamforming in wireless mobile communication systems, as well as the integration of DOA estimation in advanced technologies like MIMO systems and next-generation wireless communication systems [1], [2], [3], [4], as illustrated in Fig. 1. However, existing methods for extracting the DOA estimates are computationally complex. They invariable necessitate a large quantity of data samples (snapshots) to achieve precise DOA estimation. Additionally, as the number of antenna elements increases, as observed in massive multiple-input multiple-output (MIMO) systems, complexity increases manifold. Consequently, this places extra requirements on the real-time implementation of DOA

The associate editor coordinating the review of this manuscript and approving it for publication was Yafei Hou.

estimation algorithms, primarily due to increase in compute power and memory requirements.

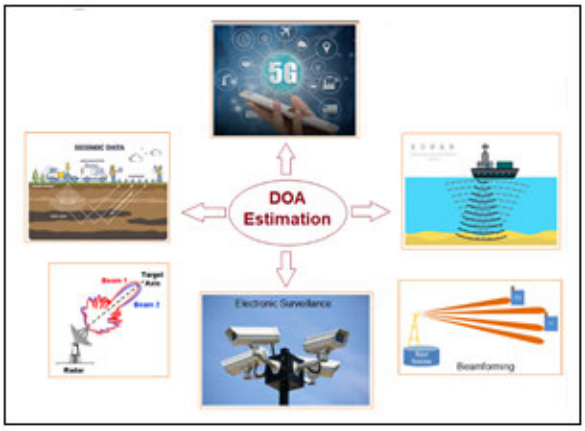

FIGURE 1. Some applications of DOA estimation.

Numerous methods exist for DOA estimation. Subspace-based DOA estimation algorithms are frequently referenced in the literature. These include widely known techniques like MUSIC [1], ESPRIT [2], as well as their various adaptations [3], [4], [5], [6]. These methods employ either Eigenvalue Decomposition (EVD) or Singular Value Decomposition (SVD) to extract the signal and noise subspaces. However, while these methods have high estimation accuracy, they have some drawbacks. These methods, along with their multiple variants [3], [4], [5], [6], [7], exhibit significant computational complexity. They require a large number of snapshots, resulting in a high computational cost (typically on the order of $O(N^3)$, where N represents the size of the received data matrix). This renders them impractical for real-time hardware implementation due to the considerably increased processing time and hardware resource requirements. Moreover, these classical DOA estimation methods perform poorly in accurately computing the DOA angle estimates when the incident signals are highly correlated or coherent [8], [9].

Improving the estimation accuracy of coherent signals has been an important research topic when addressing the challenge posed by signals in multipath environments. Typically, preprocessing steps are necessary for estimating the DOA of coherent sources, as the covariance matrix becomes singular and becomes rank deficient, rendering accurate DOA estimation of such signals very difficult [8], [9]. Specific approaches, like spatial smoothing, can be employed during the preprocessing phase to enhance the rank of the covariance matrix [10], [11], [12], [13], [14], [15], [16], [17], but their performance and computational complexity exhibit much variation. These operations add to the complexity and computation cost of DOA estimation. Moreover, the effect of spatial smoothing operations on estimation performance degrades owing to reduced array aperture [13]. Alternative techniques for decorrelation of coherent sources have been proposed which employ Toeplitz matrix theory [17], [18], [19], [20]. These techniques known as Toeplitz decorrelation techniques do not reduce array aperture and yield better performance compared to conventional spatial smoothing techniques.

Direction finding or DOA estimation along with beamforming are enabling technologies for 5G communications and beyond. However, these next generation wireless communication technologies use a very large number of antennas for providing computing, localization, sensing services (massive IoT), higher multi-Gbps peak data speeds, high throughput, and massive network capacity. The need for hundreds of antennas presents formidable challenges in DOA estimation, particularly when dealing with the computation of very large array matrices generated from the signals received by these antennas. In recent years, there have been attempts at using machine learning (ML) based methods [21], [22], [23], [24], [25] for DOA estimation which seem promising and viable. However, ML-based methods require large datasets for training these ML models to work effectively under all possible yet unpredictable real-world scenarios. Such datasets are not easy to obtain or generate. This and the inherent complexity of ML-based methods pose challenges to a wider adoption of these methods for real-time practical applications. However, it is expected that in future ML-based methods will become more efficient and feasible for deployment.

Reducing computational complexity while maintaining high estimation accuracy is critical for practical implementation in many applications such as in MIMO systems and for the next generation wireless communication systems. To this end, several approaches have been reported in the literature that avoid computationally complex EVD and SVD and have instead used computationally light matrix decomposition methods such as QR [26], LU [27], LDL [28], and Cholesky [29]. LU-based method is claimed to be superior to other methods in terms of hardware resources consumed and computation speed for FPGA hardware implementation as reported in [30]. However, they still require a large number of snapshots.

Using minimum number of snapshots of the received signals at the antenna array can significantly reduce the computational complexity of DOA estimation algorithms and make them suitable for fast real-time response as required, for instance, in the case of tracking moving targets, for sonar and in automotive radar applications. However, single snapshot-based methods suffer from performance issues and work well only at a high SNR. Several methods have been reported in the literature that proposed computing the DOA estimates using a single snapshot [31], [32], [33], [34], [35], [36], [37], [38]. However, their complexity and performance vary. More research is needed to further investigate this approach and this paper is a step in that direction.

The work reported in [31] proposes an approach that requires a pre-processing step involving covariance matrix reconstruction and manipulation of the structural information of the covariance matrix to improve DOA estimation performance using a single snapshot. This method presents

an improvement over existing methods such as root-MUSIC. However, it requires several stages of computing the DOA estimate. In the first stages, an initial estimate of the DOA is obtained which is then used in the subsequent stage which involves an iterative approach to minimize the difference between the estimated DOA and the initial DOA. While this approach improves the performance, it is inherently complex and its multistage and iterative approach increases the computation time.

R. Wu et. al. in [32] proposed methods that transform the DOA estimation task into Frobenius-norm-based optimization problems. These methods initially construct the Khatri-Rao product-like data vector, and subsequently apply a row elementary transformation to the structured data vector. While these methods have good estimation performance, they have high computational requirements.

The work presented in [33] for estimating the DOA angles from a single snapshot leverages a deterministic identification algorithm as a performance metric. This choice enhances the robustness of the DOA estimator, ensuring its ability to withstand modeling inaccuracies and noise by employing a trial-and-error approach. However, this technique has several limitations. Firstly, it is recursive in nature and is computationally intensive due to its high snapshot sampling requirements. Furthermore, it necessitates access to the physical structural details of the array to set the initial parameters. Additionally, when multiple signal sources of interest require a considerably extensive antenna array aperture, this method becomes vulnerable to estimation errors.

In the research work presented in [34], the authors introduce a single-snapshot DOA algorithm that relies on the Alternating Direction Method of Multipliers (ADMM) [39], which has been adapted to accommodate complex-valued data. ADMM is a numerical technique employed for solving convex optimization problems through iterative calculations, repeating until a specific termination condition is met or a pre-defined number of iterations is reached. The proposed method which requires sequential and iterative computation of several variables of interest, seems to have good estimation performance. However, the iterative nature of the algorithm increases computation time and makes it somewhat unpredictable.

Another method is proposed in [35] for DOA estimation using a single snapshot. This method can be applied to arbitrary array configurations and works well for both coherent and noncoherent sources. The method suggested calculates the DOA by initially transforming a multidimensional atomic norm minimization problem from the continuous angle domain into a dual maximization problem. Subsequently, the dual function is approximated as a finite trigonometric polynomial through the utilization of a truncated Fourier series. These operations increase the complexity of the proposed algorithm.

In [36], the authors introduced an algorithm based on the Matrix Pencil method. This approach involves averaging the received signal from the antenna array over N snapshots by computing the mean phase difference between the antennas. While this method improves the DOA estimation accuracy, it works only for noncoherent sources. S. Mazokha et. al. in [37] proposed an approach based on data Hankelization and singular value decomposition (SVD) to estimate the DOA angles using a single snapshot of the received data. The drawback of this method is its high computation cost due to the use of SVD.

In a different study cited in [38], an alternative multi-stage algorithm for single-snapshot DOA estimation was introduced. It begins by employing the traditional low-resolution discrete Fourier transform (DFT) spectrum to derive an initial estimate of the DOA. In the subsequent stage it refines the search region for the target DOA. However, a drawback of this technique is that it works well only when the number of antennas in a uniform linear array (ULA) exceeds 128.

Another class of DOA estimation methods that has garnered a lot of interest recently is based on the compressed sensing (CS) technique [40], [41], [42], [43], [44], [45], [46], [47], [48] which exploits signal sparsity to reduce the number of required measurements, aiming to achieve accurate angle estimation with fewer snapshots. However, some CS-based methods such as l1-norm minimization [44], [45], [46] or iterative methods [47], [48] can be computationally intensive. The complexity might also increase with larger problem sizes or higher levels of sparsity. Another drawback of CS-based methods is that convergence of iterative algorithms used in CS may require multiple iterations to reconstruct sparse signals accurately, leading to longer computation times, especially for signals with lower sparsity levels. Moreover, achieving real-time CS-based DOA estimation might be challenging due to the computational demands of the reconstruction algorithms, especially in scenarios where rapid and continuous estimation is required.

In this paper, we address two main challenges facing DOA estimation – 1) increasing computational complexity for large antenna arrays (such as for MIMO systems) using multiple snapshots of received signals which require the processing of extensive array matrices generated from signals received by hundreds of antennas, 2) accurate estimation of highly correlated sources without increasing computational complexity. In an attempt to address these challenges, we propose in this paper a new low complexity algorithm that accurately estimates the DOA of multiple coherent signals using only a single snapshot from a uniform linear array (ULA). First, a single snapshot of the received signals at the antenna array is used to construct a Toeplitz structure matrix. The complex-valued Toeplitz matrix is converted to a real-valued matrix using a novel method which does not require unitary transformations. QR decomposition method is used to extract the signal and noise subspaces. The noise subspace is utilized in the subsequent steps based on polynomial rooting to obtain the DOA estimates. Use of real-valued matrices reduces complexity of matrix operations by a factor of four.

Prior to deployment, it is of vital importance to validate DOA estimation algorithms experimentally for real-time response under realistic scenarios. Majority of the work reported in the literature validated algorithms only numerically using computer simulations. A few works have looked at experimental validation of DOA estimation algorithms on different hardware platforms [49], [50], [51], [52], [53], [54], [55]. Owing to its practical significance, the performance of the proposed method has been validated through real-time experiments on a software defined radio platform using NI USRPs and LabVIEW, in addition to computer simulations using MATLAB. The following are the advantages of the proposed method:

- Requires only a single snapshot to yield accurate estimation.
- Does not require computationally complex EVD/SVD.
- Does not require the covariance matrix to be computed.
- Has low complexity and fast computation time.
- It works well for both noncoherent and coherent sources.
- Converts complex-valued data to real-valued data using a novel method.
- Works with real-valued data reducing computation cost by a factor of 4.
- Highly suitable for practical real-time implementations.
- Highly suitable for use in MIMO systems and next generation wireless communication systems.

The rest of this paper is organized as follows: Section II presents the system model and the proposed algorithm; Section III analyses the computational complexity of the proposed algorithm in comparison with the unitary root-MUSIC method; Section IV presents the MATLAB simulation results; Section V describes the prototype testbed using a 9-element ULA for real-time experimental validation; and Section VI presents the results of real-time experiments on the prototype testbed; the paper ends with conclusions in Section VII.

II. SYSTEM MODEL AND PROPOSED ALGORITHM

The system model is built around a centro-symmetric uniform linear array (ULA) consisting of $2N + 1$ receiving antennas. The antenna element in the center of the array is considered as the reference position (#0). This leaves N antenna elements on either side of the reference position, as shown in Fig. 2. The separation between antenna elements, d, is equal to half the wavelength of incident signals. The signals whose DOAs are to be estimated are considered to be in the far-field region of the antenna array.

Consider K narrowband source signals impinging on the array at angles of incidence $(\theta_1\theta_2, \ldots \theta_K)$, with $K < 2N + 1$. It is assumed that all incident sources have the same carrier frequency. The output signal from the n^{th} element on the ULA for a given snapshot at time t is given by:

$$y_n(t) = \sum_{i=1}^{K} e^{-j\left(\frac{2\pi}{\lambda}(n)\right)dcos\theta_i} s_i(t) + n_n(t) \tag{1}$$

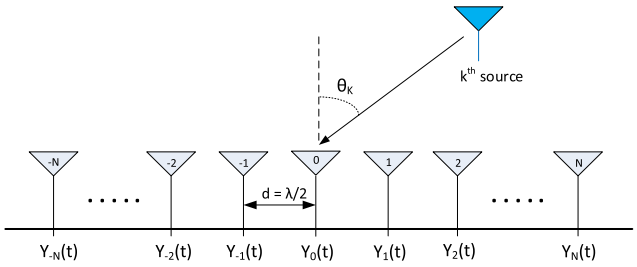

FIGURE 2. Centro-symmetric uniform linear array with 2N+1 elements.

where

$s_i(t)$ = ith source signal incident on the ULA,

$n_n(t)$ = additive white Gaussian noise (AWGN) at the nth element,

$y_n(t)$ = received signal at the nth element at time t where $-N \leq n \leq N$.

Taking the element at the center of the array as the reference point, we can express the output vector from the $(2N+1)$ antenna elements positioned along the linear axis as follows:

$$\widehat{\boldsymbol{Y}}(t) = \begin{bmatrix} Y_{-N}(t) \\ \vdots \\ Y_0(t) \\ \vdots \\ Y_N(t) \end{bmatrix} = \boldsymbol{A}(\theta)\, s(t) + n(t) \tag{2}$$

where dimension of $\boldsymbol{Y}(t)$ is $(2N+1)$ x 1, and

$$\boldsymbol{A}(\theta) = \left[a(\theta_1)\ a(\theta_2)\ \ldots\ a(\theta_K) \right] \tag{3}$$

is the array response matrix of dimension $(2N + 1) \times K$, where

$$a(\theta_k) = \left[(u_k^*)^N \ \cdots\ 1 \ \cdots\ u_k^N \right]^T \tag{4}$$

is the corresponding array transfer vector of size $(2N+1) \times 1$, where

$$u_k = e^{-j\left(\frac{2\pi}{\lambda}\right)dcos(\theta_k)} \tag{5}$$

s(t) is the vector of K received signals

$$s(t) = [s_1(t)\ s_2(t)\ \cdots s_K(t)]^T \tag{6}$$

and,

$$\mathrm{n}(t) = \left[\left(n_{-N}(t) \cdots\ n_0(t)\ \cdots n_N(t)\ \right) \right]^T \tag{7}$$

where

$\mathrm{n}(t)$ is the noise vector of size $(2N + 1) \times 1$. The superscripts $(\cdot)^H$, $(\cdot)^T$, and $(\cdot)^*$, denote the Hermitian, transpose, and conjugate operations, respectively.

In the proposed method, first we average the received signal data vectors $Y(t)$ over L samples, as:

$$z(t) = \frac{1}{L}\sum_{i=1}^{L}\widehat{Y}_i(t) = \begin{bmatrix} z_{-N}(t) \\ \vdots \\ z_0(t) \\ \vdots \\ z_N(t) \end{bmatrix} \tag{8}$$

Next, we construct the Toeplitz structure data matrix $\boldsymbol{Z}$ with dimension $(N+1)\times(N+1)$ using the sample-averaged data vector z(t) as follows:

$$\begin{aligned} \boldsymbol{Z} &= \begin{bmatrix} z_0 & z_{-1} & & z_{-N} \\ z_1 & z_0 & \cdots & z_{-(N-1)} \\ z_2 & z_1 & & z_{-(N-2)} \\ \vdots & \vdots & \ddots & \vdots \\ z_N & z_{N-1} & \cdots & z_0 \end{bmatrix} \\ &= \begin{bmatrix} x_0 & x_{-1} & & x_{-N} \\ x_1 & x_0 & \cdots & x_{-(N-1)} \\ x_2 & x_1 & & x_{-(N-2)} \\ \vdots & \vdots & \ddots & \vdots \\ x_N & x_{N-1} & \cdots & x_0 \end{bmatrix} \\ &+ \begin{bmatrix} n_0 & n_{-1} & & n_{-N} \\ n_1 & n_0 & \cdots & n_{-(N-1)} \\ n_2 & n_1 & & n_{-(N-2)} \\ \vdots & \vdots & \ddots & \vdots \\ n_N & n_{N-1} & \cdots & n_0 \end{bmatrix} \end{aligned} \tag{9}$$

where

x_i = source signal component at the ith element of the ULA

n_i = noise signal component at the ith element of the ULA

Considering the noiseless case for the sake of simplicity, the Toeplitz structure matrix $\boldsymbol{Z}$ can be decomposed according to the Vandermonde decomposition theorem [56], as:

$\boldsymbol{Z} = \tilde{\boldsymbol{A}}\boldsymbol{S}_p\tilde{\boldsymbol{A}}^H$

In the presence of noise, we have:

$$\boldsymbol{Z} = \boldsymbol{Z}_x(t) + \boldsymbol{Z}_n(t) = \tilde{\boldsymbol{A}}\boldsymbol{S}_p\tilde{\boldsymbol{A}}^H + \tilde{\boldsymbol{A}}\boldsymbol{N}_p\tilde{\boldsymbol{A}}^H \tag{10}$$

where $\tilde{\boldsymbol{A}} = [\tilde{\boldsymbol{A}}(\theta_1)\ \tilde{\boldsymbol{A}}(\theta_2)\ \cdots\ \tilde{\boldsymbol{A}}(\theta_K)]$ is the $(N+1)$ x K Vandermonde array steering matrix with $\tilde{\boldsymbol{A}}(\theta_k) = \left[1 e^{-j\left(\frac{2\pi}{\lambda}\right)dcos(\theta_k)} \ldots e^{-j\left(\frac{2\pi}{\lambda}\right)Ndcos(\theta_k)}\right]^T$, $\boldsymbol{S}_p = \text{diag}[s_1, \ldots, s_K]$ is a positive definite diagonal matrix with dimension K x K where $s_k > 0$ (k = 1, …, K) are the incident signal sources, and $\boldsymbol{N}_p = \text{diag}[n_1, \ldots, n_K]$ is diagonal matrix of noise signals. The Vandermonde decomposition theorem first introduced in [57] is stated below:

Theorem: Any positive semidefinite (PSD) Toeplitz matrix $T(x) \in C^{NxN}$ of rank $r \le N$ admits the following r-atomic Vandermonde decomposition:

$$\boldsymbol{T} = \boldsymbol{A}\boldsymbol{S}\boldsymbol{A}^H$$

where $S = diag(s_1, \ldots, s_k)$ is an $K \times K$ positive definite diagonal matrix of signal powers and A is an $N \times K$ Vandermonde matrix.

Analysis: Consider two sources $s_1(t)$ and $s_2(t)$ impinging on a 5-element ULA. For the sake of simplicity and constraint of space, consider noiseless signals.

Let

Hence, $\boldsymbol{Z} = \tilde{\boldsymbol{A}}\boldsymbol{S}_p\tilde{\boldsymbol{A}}^H$.

Likewise, in the presence of noise, it can be shown that $\boldsymbol{Z} = \tilde{\boldsymbol{A}}\boldsymbol{S}_p\tilde{\boldsymbol{A}}^H + \tilde{\boldsymbol{A}}\boldsymbol{N}_p\tilde{\boldsymbol{A}}^H$

The Vandermonde decomposition, a foundational finding attributed to Caratheodory and Fejér in 1911 [57], has garnered significance within the realms of data analysis and signal processing. Its prominence has grown since the 1970s, following its rediscovery by Pisarenko, who harnessed it for the purpose of extracting frequencies from the data covariance matrix [58].

Since $\boldsymbol{Z} = \tilde{\boldsymbol{A}}\boldsymbol{S}_p\tilde{\boldsymbol{A}}^H$ and the diagonal signal matrix $\boldsymbol{S}_p$ is of full rank, the rank of $\boldsymbol{Z}$ is the same as that of $\tilde{\boldsymbol{A}}$. The matrix $\tilde{\boldsymbol{A}}$ in (9) has the structure of a Vandermonde matrix and its rank cannot exceed K; hence, rank of $\boldsymbol{Z}$ is equal to K. This means that the rank of the Hermitian Toeplitz data matrix $\boldsymbol{Z}$ is equal to the number of sources whose DOAs are to be estimated, regardless of the sources being non-coherent or highly correlated. Therefore, DOAs of all the incident sources can be successfully estimated because the Toep1itz data matrix structure is preserved in either scenario (i.e., coherent or non-coherent sources).

Since the real-time data is noisy and the noise is random at each of the antenna elements in the array, the off-diagonal elements of Z are not conjugate of each other. For example, the off-diagonal noise matrix elements n_{-1} and n_1 in (9) are not equal ($n_{-1} \neq n_1*$). In preparation for converting the complex-valued matrix $\boldsymbol{Z}$ to a real-valued one, we apply a conjugate smoothing operation (CSO) by adding $\boldsymbol{Z}$ to its Hermitian keeping the Toeplitz structure of the matrix unchanged even in the presence of noise.

$$\widehat{\boldsymbol{Z}} = \frac{1}{2}(\boldsymbol{Z} + \boldsymbol{Z}^{\boldsymbol{H}}) = \frac{\boldsymbol{1}}{\boldsymbol{2}}(\boldsymbol{Z} + \boldsymbol{J}\boldsymbol{Z}^*\boldsymbol{J}) \tag{11}$$

where $\boldsymbol{J}$ is $(N+1)\times(N+1)$ matrix with ones in the off-diagonal elements and zeros elsewhere.

The operation in (11) is equivalent to the forward-backward averaging of the data matrix $\boldsymbol{Z}$ to produce $\widehat{\boldsymbol{Z}}$.

Analysis: Consider the two sources $s_1(t)$ and $s_2(t)$ to be coherent ($s_1(t) = s_2(t) = s(t)$). In the presence of noise, $\boldsymbol{Z}$ can be expressed as: shown in the equation at the bottom of the next page.

Let $e^{j\alpha_1} + e^{j\alpha_2} = cos\alpha_1 + jsin\alpha_1 + cos\alpha_2 + jsin\alpha_2 = \mu_1 + j\gamma_1$

where $\mu_1 = cos\alpha_1 + cos\alpha_2$ and $\gamma_1 = sin\alpha_1 + sin\alpha_2$

and $e^{j2\alpha_1} + e^{j2\alpha_2} = cos2\alpha_1 + jsin2\alpha_1 + cos2\alpha_2 + jsin2\alpha_2 = \mu_2 + j\gamma_2$

where $\mu_2 = cos2\alpha_1 + cos2\alpha_2$ and $\gamma_2 = sin2\alpha_1 + sin2\alpha_2$

Similarly,

$$e^{-j\alpha_1} + e^{-j\alpha_2} = cos\alpha_1 - jsin\alpha_1 + cos\alpha_2 - jsin\alpha_2 = \mu_1 - j\gamma_1$$

$$e^{-j2\alpha_1}+e^{-j2\alpha_2}=cos2\alpha_1-jsin2\alpha_1+cos2\alpha_2-jsin2\alpha_2$$
$$=\mu_2-j\gamma_2$$

Matrix $\boldsymbol{Z}$ can now be rewritten as: shown in the equation at the bottom of the next page.

Now, the off-diagonal elements of $\widehat{\boldsymbol{Z}}$ are conjugate of each other. For example, $\widehat{\boldsymbol{Z}}_{21}=\widehat{\boldsymbol{Z}}_{12}^{*}$

Next, it will be shown that $\boldsymbol{JZ^*J}=\boldsymbol{Z^H}$

Let

$$\boldsymbol{Z}=\begin{bmatrix} z_0 & z_{-1} & z_{-2} \\ z_1 & z_0 & z_{-1} \\ z_2 & z_1 & z_0 \end{bmatrix} \Longrightarrow \boldsymbol{Z^H}=\begin{bmatrix} z_0^* & z_1^* & z_2^* \\ z_{-1}^* & z_0^* & z_1^* \\ z_{-2}^* & z_{-1}^* & z_0^* \end{bmatrix}$$

$$\boldsymbol{JZ^*J}=\begin{bmatrix} 0 & 0 & 1 \\ 0 & 1 & 0 \\ 1 & 0 & 0 \end{bmatrix}\begin{bmatrix} z_0^* & z_{-1}^* & z_{-2}^* \\ z_1^* & z_0^* & z_{-1}^* \\ z_2^* & z_1^* & z_0^* \end{bmatrix}\begin{bmatrix} 0 & 0 & 1 \\ 0 & 1 & 0 \\ 1 & 0 & 0 \end{bmatrix}$$
$$=\begin{bmatrix} 0 & 0 & 1 \\ 0 & 1 & 0 \\ 1 & 0 & 0 \end{bmatrix}\begin{bmatrix} z_{-2}^* & z_{-1}^* & z_0^* \\ z_{-1}^* & z_0^* & z_1^* \\ z_0^* & z_1^* & z_2^* \end{bmatrix}$$
$$=\begin{bmatrix} z_0^* & z_1^* & z_2^* \\ z_{-1}^* & z_0^* & z_1^* \\ z_{-2}^* & z_{-1}^* & z_0^* \end{bmatrix}=\boldsymbol{Z^H}$$

Thus, $\boldsymbol{JZ^*J}=\boldsymbol{Z^H}$ **and** $\boldsymbol{Z}+\boldsymbol{Z^H}=\boldsymbol{Z}+\boldsymbol{JZ^*J}$

Next, in the proposed algorithm a novel method [59] is developed to convert the complex-valued data matrix $\widehat{\boldsymbol{Z}}$ in (11) into a real matrix without any additional signal processing steps, as:

$$\widehat{\boldsymbol{Z}}_{\boldsymbol{r}}=\text{real}\left(\widehat{\boldsymbol{Z}}\right)+\text{imag}\left(\widehat{\boldsymbol{Z}}\right)*\boldsymbol{J}=\mathbf{T}+\mathbf{H} \tag{12}$$

where $\mathbf{T}$ is a symmetric Toeplitz matrix, $\mathbf{H}$ is a Hankel skew-centrosymmetric matrix, and $\boldsymbol{J}$ is $(N+1)\times(N+1)$ matrix with ones in the off-diagonal elements and zeros elsewhere.

The conversion of complex-valued data to real data using this novel method is illustrated in the following numerical example.

Example:

Let

$$\widehat{\boldsymbol{Z}}=\begin{bmatrix} 8 & 3+j2 & 5+j7 & 4+j \\ 3-j2 & 8 & 3-j2 & 5-j7 \\ 5-j7 & 3+j2 & 8 & 3-j2 \\ 4-j & 5+j7 & 3+j2 & 8 \end{bmatrix}$$

$$\widehat{Z}_r=\begin{bmatrix} 8 & 3 & 5 & 4 \\ 3 & 8 & 3 & 5 \\ 5 & 3 & 8 & 3 \\ 4 & 5 & 3 & 8 \end{bmatrix}+j\begin{bmatrix} 0 & 2 & 7 & 1 \\ -2 & 0 & 2 & 7 \\ -7 & -2 & 0 & 2 \\ -1 & -7 & -2 & 0 \end{bmatrix}*\boldsymbol{J}$$

$$\alpha_1=\frac{2\pi d cos\theta_1}{\lambda};\alpha_2=\frac{2\pi d cos\theta_2}{\lambda};\boldsymbol{S}_p=\begin{bmatrix} s_1(t) & 0 \\ 0 & s_2(t) \end{bmatrix}$$
$$x_0=s_1(t)+s_2(t)$$
$$x_1=e^{-j\alpha_1}s_1(t)+e^{-j\alpha_2}s_2(t)$$
$$x_{-1}=e^{j\alpha_1}s_1(t)+e^{j\alpha_2}s_2(t)$$
$$x_2=e^{-j2\alpha_1}s_1(t)+e^{-j2\alpha_2}s_2(t)$$
$$x_{-2}=e^{j2\alpha_1}s_1(t)+e^{j2\alpha_2}s_2(t)$$
$$\tilde{\boldsymbol{A}}(\theta)=\begin{bmatrix} 1 & 1 \\ e^{-j\alpha_1} & e^{-j\alpha_2} \\ e^{-j2\alpha_1} & e^{-j2\alpha_2} \end{bmatrix};\tilde{\boldsymbol{A}}^{\boldsymbol{H}}(\theta)=\begin{bmatrix} 1 & e^{j\alpha_1} & e^{j2\alpha_1} \\ 1 & e^{j\alpha_2} & e^{j2\alpha_2} \end{bmatrix}$$
$$\boldsymbol{Z}=\begin{bmatrix} x_0 & x_{-1} & x_{-2} \\ x_1 & x_0 & x_{-1} \\ x_2 & x_1 & x_0 \end{bmatrix}$$
$$=\begin{bmatrix} s_1(t)+s_2(t) & e^{j\alpha_1}s_1(t)+e^{j\alpha_2}s_2(t) & e^{j2\alpha_1}s_1(t)+e^{j2\alpha_2}s_2(t) \\ e^{-j\alpha_1}s_1(t)+e^{-j\alpha_2}s_2(t) & s_1(t)+s_2(t) & e^{j\alpha_1}s_1(t)+e^{j\alpha_2}s_2(t) \\ e^{-j2\alpha_1}s_1(t)+e^{-j2\alpha_2}s_2(t) & e^{-j\alpha_1}s_1(t)+e^{-j\alpha_2}s_2(t) & s_1(t)+s_2(t) \end{bmatrix}$$

$$\tilde{\boldsymbol{A}}\boldsymbol{S}_p\tilde{\boldsymbol{A}}^H=\begin{bmatrix} 1 & 1 \\ e^{-j\alpha_1} & e^{-j\alpha_2} \\ e^{-j2\alpha_1} & e^{-j2\alpha_2} \end{bmatrix}\begin{bmatrix} s_1(t) & 0 \\ 0 & s_2(t) \end{bmatrix}\begin{bmatrix} 1 & e^{j\alpha_1} & e^{j2\alpha_1} \\ 1 & e^{j\alpha_2} & e^{j2\alpha_2} \end{bmatrix}=\begin{bmatrix} s_1(t) & s_2(t) \\ e^{-j\alpha_1}s_1(t) & e^{-j\alpha_2}s_2(t) \\ e^{-j2\alpha_1}s_1(t) & e^{-j2\alpha_2}s_2(t) \end{bmatrix}\begin{bmatrix} 1 & e^{j\alpha_1} & e^{j2\alpha_1} \\ 1 & e^{j\alpha_2} & e^{j2\alpha_2} \end{bmatrix}$$
$$=\begin{bmatrix} s_1(t)+s_2(t) & e^{j\alpha_1}s_1(t)+e^{j\alpha_2}s_2(t) & e^{j2\alpha_1}s_1(t)+e^{j2\alpha_2}s_2(t) \\ e^{-j\alpha_1}s_1(t)+e^{-j\alpha_2}s_2(t) & s_1(t)+s_2(t) & e^{j\alpha_1}s_1(t)+e^{j\alpha_2}s_2(t) \\ e^{-j2\alpha_1}s_1(t)+e^{-j2\alpha_2}s_2(t) & e^{-j\alpha_1}s_1(t)+e^{-j\alpha_2}s_2(t) & s_1(t)+s_2(t) \end{bmatrix}$$

$$\boldsymbol{Z}=\begin{bmatrix} 2s(t)+n_0(t) & (e^{j\alpha_1}+e^{j\alpha_2})s(t)+n_{-1}(t) & (e^{j2\alpha_1}+e^{j2\alpha_2})s(t)+n_{-2}(t) \\ (e^{-j\alpha_1}+e^{-j\alpha_2})s(t)+n_1(t) & 2s(t)+n_0(t) & (e^{j\alpha_1}+e^{j\alpha_2})s(t)+n_{-1}(t) \\ (e^{-j2\alpha_1}+e^{-j2\alpha_2})s(t)+n_2(t) & (e^{-j\alpha_1}+e^{-j\alpha_2})s(t)+n_1(t) & 2s(t)+n_0(t) \end{bmatrix}$$

$$\widehat{\boldsymbol{Z}}_r = \begin{bmatrix} 8 & 3 & 5 & 4 \\ 3 & 8 & 3 & 5 \\ 5 & 3 & 8 & 3 \\ 4 & 5 & 3 & 8 \end{bmatrix} + \begin{bmatrix} 0 & 2 & 7 & 1 \\ -2 & 0 & 2 & 7 \\ -7 & -2 & 0 & 2 \\ -1 & -7 & -2 & 0 \end{bmatrix} \times \begin{bmatrix} 0 & 0 & 0 & 1 \\ 0 & 0 & 1 & 0 \\ 0 & 1 & 0 & 0 \\ 1 & 0 & 0 & 0 \end{bmatrix}$$

$$\widehat{\boldsymbol{Z}}_r = \begin{bmatrix} 8 & 3 & 5 & 4 \\ 3 & 8 & 3 & 5 \\ 5 & 3 & 8 & 3 \\ 4 & 5 & 3 & 8 \end{bmatrix} + \begin{bmatrix} 1 & 7 & 2 & 0 \\ 7 & 2 & 0 & -2 \\ 2 & 0 & -2 & -7 \\ 0 & -2 & -7 & -1 \end{bmatrix} = \begin{bmatrix} 9 & 10 & 7 & 4 \\ 10 & 10 & 3 & 3 \\ 7 & 3 & 6 & -4 \\ 4 & 3 & -4 & 7 \end{bmatrix}$$

The above novel method of converting a complex-valued matrix to a real-valued matrix takes fewer operations compared with the unitary transformation method. The advantage of converting the complex-valued matrix to a real-valued matrix is that it reduces the computation time by a factor of four and memory resources consumption by a factor of two. For subsequent steps in the proposed algorithm for computing the DOA estimates, using a real-valued matrix reduces the computation cost by a factor of at least four.

In the next step, the signal and noise subspaces are extracted from $\widehat{\boldsymbol{Z}}_r$ by using QR decomposition method.

$$\mathrm{QR}(\widehat{\boldsymbol{Z}}_r) = \begin{bmatrix} \boldsymbol{Q}_s & \boldsymbol{Q}_n \end{bmatrix} \begin{bmatrix} \boldsymbol{R}_s \\ \vdots \\ \boldsymbol{O} \end{bmatrix} \tag{13}$$

where

$\boldsymbol{Q}_s$ = signal space matrix of size $(N+1) \times K$,
$\boldsymbol{Q}_n$ = noise space matrix of size $(N+1) \times ((N+1)\text{-}K)$,
$\boldsymbol{R}_s$ = upper triangular signal space matrix of size $(K \times N+1)$,
$\boldsymbol{O}$ = lower triangular matrix of size $((N+1)\text{-}K) \times (N+1)$ with all elements as zeros.

The column vectors of matrix $\boldsymbol{Q}$ form an orthonormal basis. The noise subspace matrix $\boldsymbol{Q}_n$ is used to compute the power spectrum $\boldsymbol{P}(\theta)$ similar to the MUSIC method.

$$\boldsymbol{P}(\theta) = \frac{1}{\boldsymbol{U}\tilde{\boldsymbol{A}}(\theta)^H (\boldsymbol{Q}_n \boldsymbol{Q}_n^H) \tilde{\boldsymbol{A}}(\theta)\, \boldsymbol{U}^H} \tag{14}$$

where $\boldsymbol{U}$ is a unitary matrix with dimensions $(N+1) \times (N+1)$.

$$\boldsymbol{U} = \boldsymbol{I}j + \boldsymbol{J} = \begin{bmatrix} j & 0 & 0 & \cdots & 1 \\ 0 & j & 1 & \cdots & 0 \\ 0 & \vdots & \vdots & \cdots & 0 \\ \vdots & 1 & j & \ddots & \\ 1 & 0 & 0 & \cdots & j \end{bmatrix} \tag{15}$$

where $\boldsymbol{I}$ is the identity matrix and $\boldsymbol{J}$ is a matrix with ones in the off diagonal elements and zeros elsewhere, both of dimension $(N+1) \times (N+1)$.

As indicated in equation (14), we can determine the DOA of incoming signals by performing a 1D spectrum peak search across the range of θ. To further decrease computational complexity, we can adjust the spectrum search in equation (14) to compute DOAs using polynomial roots. The modified estimator can be defined as follows:

Assuming $w = exp\left(\frac{-j2\pi d cos(\theta_k)}{\lambda}\right)$, we can rewrite $\tilde{\boldsymbol{A}}(\theta_k)$ as:

$$\boldsymbol{a}(w) = \begin{bmatrix} 1 & w & \ldots & w^N \end{bmatrix}^T \tag{16}$$

$$\boldsymbol{Z} = \begin{bmatrix} 2s(t) + n_0(t) & (\mu_1 + j\gamma_1)s(t) + n_{-1}(t) & (\mu_2 + j\gamma_2)s(t) + n_{-2}(t) \\ (\mu_1 - j\gamma_1)s(t) + n_1(t) & 2s(t) + n_0(t) & (\mu_1 + j\gamma_1)s(t) + n_{-1}(t) \\ (\mu_2 - j\gamma_2)s(t) + n_2(t) & (\mu_1 - j\gamma_1)s(t) + n_1(t) & 2s(t) + n_0(t) \end{bmatrix}$$

$$\boldsymbol{Z}^{\boldsymbol{H}} = \begin{bmatrix} 2s^*(t) + n_0^*(t) & (\mu_1 + j\gamma_1)s^*(t) + n_1^*(t) & (\mu_2 + j\gamma_2)s^*(t) + n_2^*(t) \\ (\mu_1 - j\gamma_1)s^*(t) + n_{-1}^*(t) & 2s^*(t) + n_0^*(t) & (\mu_1 + j\gamma_1)s^*(t) + n_1(t) \\ (\mu_2 - j\gamma_2)s^*(t) + n_{-2}^*(t) & (\mu_1 - j\gamma_1)s^*(t) + n_{-1}^*(t) & 2s^*(t) + n_0^*(t) \end{bmatrix}$$

$$\therefore \widehat{\boldsymbol{Z}} = \boldsymbol{Z} + \boldsymbol{Z}^{\boldsymbol{H}} = \begin{bmatrix} 2(s(t) + s^*(t)) + n_0(t) + n_0^*(t) & (\mu_1 + j\gamma_1)(s(t) + s^*(t)) + n_{-1}(t) + n_1^*(t) & (\mu_2 + j\gamma_2)(s(t) + s^*(t)) + n_{-2}(t) + n_2^*(t) \\ (\mu_1 - j\gamma_1)(s(t) + s^*(t)) + n_1(t) + n_{-1}^*(t) & 2(s(t) + s^*(t)) + n_0(t) + n_0^*(t) & (\mu_1 + j\gamma_1)(s(t) + s^*(t)) + n_{-1}(t) + n_1^*(t) \\ (\mu_2 - j\gamma_2)(s(t) + s^*(t)) + n_2(t) + n_{-2}^*(t) & (\mu_1 - j\gamma_1)(s(t) + s^*(t)) + n_1(t) + n_{-1}^*(t) & 2(s(t) + s^*(t)) + n_0(t) + n_0^*(t) \end{bmatrix}$$

The denominator in (14) expressed in polynomial form:

$$f(w) = \boldsymbol{U}\tilde{\boldsymbol{A}}^{H}(w)\boldsymbol{Q}_n\boldsymbol{Q}_n^{H}\tilde{\boldsymbol{A}}\,(w)\,\boldsymbol{U}^{H} \tag{17}$$

Like root-MUSIC, the roots z_k of the polynomial function in (17) can be used to calculate the DOAs of the incident sources as follows:

$$\theta_k = arccos\left(\frac{\lambda angle\,(w_k)}{2\pi d}\right) \tag{18}$$

The following steps summarize the proposed method:

Step 1: Construct the Toeplitz structure data matrix $\boldsymbol{Z}$ using the sample-averaged data vector z(t)

Step 2: Compute $\widehat{\boldsymbol{Z}}$ as in (11)

Step 3: Convert the complex-valued data matrix $\widehat{\boldsymbol{Z}}$ to a real-valued matrix $\widehat{\boldsymbol{Z}}_{\boldsymbol{r}}$ as in (12)

Step 4: Extract the signal and noise subspaces from $\widehat{\boldsymbol{Z}}_{\boldsymbol{r}}$ using QR decomposition as in (14)

Step 5: Compute the roots of the polynomial in (18)

Step 6: Compute the DOAs according to (19)

In this paper, the proposed method is compared with an existing method called unitary root-MUSIC (URM) [60] which is a real-valued search-free variant of the popular and classical subspace-based DOA estimation algorithm MUSIC.

In URM, a covariance matrix of size N x N is computed from a large number of data samples as:

$$\boldsymbol{R} = \frac{1}{L}\sum_{k=1}^{L} Y(k)Y^{H}(k) \tag{19}$$

In comparison, the proposed method can accurately estimate the DOAs from a single snapshot, thus, significantly reducing the complexity.

Next, forward-backward averaging smoothing (FBSS) operation is applied to the covariance matrix as:

$$\boldsymbol{R_{FB}} = \frac{1}{2}(\boldsymbol{R} + \boldsymbol{JR^{*}J}) \tag{20}$$

where $\boldsymbol{J}$ is N x N matrix with ones in the off diagonal elements and zeros elsewhere.

In order to convert the complex-valued $\boldsymbol{R_{FB}}$ to a real-valued matrix, it is left- and right-multiplied by a unitary transformation matrix $\boldsymbol{U_u}$ as:

$$\widehat{\boldsymbol{R}}_R = \boldsymbol{U}_{\boldsymbol{u}}^{H}\boldsymbol{R_{FB}}\boldsymbol{U_u} \tag{21}$$

where

$$\begin{aligned}\boldsymbol{U_u} &= \frac{1}{\sqrt{2}}\begin{bmatrix}\boldsymbol{I}_M & i\boldsymbol{I}_M \\ \boldsymbol{J}_M & -i\boldsymbol{J}_M\end{bmatrix}\boldsymbol{U_u} \\ &= \frac{1}{\sqrt{2}}\begin{bmatrix}\boldsymbol{I}_M & \boldsymbol{O_{Mx1}} & i\boldsymbol{I}_M \\ \boldsymbol{O_{1xM}} & \sqrt{2} & \boldsymbol{O_{1xM}} \\ \boldsymbol{J}_M & \boldsymbol{O_{Mx1}} & -i\boldsymbol{J}_M\end{bmatrix}\end{aligned} \tag{22}$$

where $M = N/2$ for even N, and $M = (N\text{-}1)/2$ for odd N.

Conversion from complex-valued to real-valued data matrix in the proposed method is less complex and takes fewer operations compared with the one in (21) for URM.

Next, the signal and noise subspaces are extracted by applying eigenvalue decomposition to the real-valued matrix $\widehat{\boldsymbol{R}}_R$. In contrast, the proposed method uses QR decomposition resulting in lower complexity and computation cost since QR requires $O(2N^3/3)$ operations whereas EVD requires $O(N^3)$ operations. Another drawback of applying EVD in the existing methods such as URM is that complex eigenvalues may cause the real matrix obtained by applying the unitary transformation in (21) to revert to a complex-valued matrix again since complex eigenvalues will yield complex eigenvectors.

The subsequent steps in URM are similar to the root-MUSIC method which involves polynomial rooting and finally computing the DOAs.

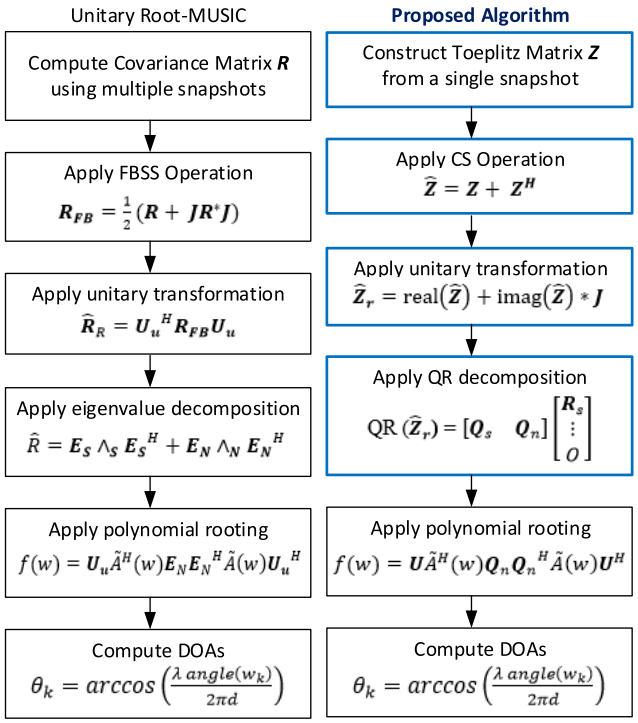

FIGURE 3. Flowcharts of URM and proposed algorithms.

Fig. 3 illustrates the major steps involved in computing the DOA estimates using the URM and the proposed algorithm. For the proposed method, the Toeplitz matrix $\boldsymbol{Z}$ is constructed using the sample-averaged data vector z(t) as shown in (9). The next section will analyze the computational complexity of the proposed algorithm and URM and show why the proposed method is superior in terms of lower computation cost.

III. COMPLEXITY ANALYSIS

In this section, we delve into the computational complexity of the proposed algorithm (PM) and unitary root-MUSIC (URM). We will show why the proposed method outperforms URM in terms of the computational cost associated with obtaining DOA estimates. Our analysis considers K signal sources, $2N + 1$ antenna elements, and L snapshots as parameters for formulating the cost equations. Table 1

TABLE 1. Computational cost for proposed method and unitary Root-MUSIC for major signal processing steps for DOA estimation.

Signal Processing Step	PM	Signal Processing Step	URM
Data vector averaging over L samples	$(2N+1)(L-1)$	Compute Covariance Matrix for L snapshots	$(L+1)(2N+1)^2$
Toeplitz structure preservation	$(N+1)^2$	Forward-backward averaging	$3(2N+1)^2$
Unitary transformation	$2(N+1)^2$	Unitary transformation	$4(2N+1)^2$
QR Decomposition	$2(N+1)^3/3$	Eigenvalue Decomposition	$2(2N+1)^3$
Matrix multiplication	$(N+1)^3 + K(N+1)^2$	Matrix multiplication	$(2N+1)^3 + K(2N+1)^2$
Compute Polynomial Roots	$2N(N+1)^2$	Compute Polynomial Roots	$4N(2N+1)^2$
Compute DOAs	$2N$	Compute DOAs	$4N$

TABLE 2. Computational cost with varying N.

N	PM	URM	% $(\frac{PM}{URM})$	N	URM_2	% $(\frac{PM}{URM2})$
8	3030	27776	10.91	4	4552	66.56
16	19235	191728	10.03	8	27776	69.25
24	59889	614752	9.74	12	85048	70.42
32	136254	1419728	9.60	16	191728	71.07
48	441177	4667056	9.45	24	614752	71.76
64	1024115	10916752	9.38	32	1419728	72.13
128	7938270	85600016	9.27	64	10916752	72.72
256	62505395	677924368	9.22	128	85600016	73.02

presented below provides a breakdown of the computational costs for the major signal processing steps for both the proposed method and the URM.

For a numerical comparison of computation cost for the proposed method with URM, we calculate the total number of arithmetic operations for the case of $K = 3$, $L = 2$, and N varying from 8 to 256, as listed in Table 2 below. It is to be recalled that number of antenna elements is equal to $2N+1$.

Table 2 clearly illustrates the superiority of the proposed method, which requires significantly fewer operations when compared to the unitary root-MUSIC method. Specifically, the proposed method requires only around 10% of the operations that URM does. Furthermore, this percentage decreases as the number of antenna elements increases, starting at 10.9%. This makes the proposed method highly suitable for practical real-time applications and its deployment in MIMO systems. In column 6 of Table 2, we also calculate the number of operations required for URM when the number of antenna elements is halved and compare it with the values for PM in column 2. Even with twice the number of antenna elements, the proposed method only requires roughly 70% of the operations necessary for URM.

IV. MATLAB SIMULATION RESULTS

This section presents the results from several MATLAB simulations conducted to thoroughly investigate the performance of the proposed method and help verify and establish its estimation accuracy under different simulation scenarios. The performance of the proposed method is examined by calculating RMSE values against varying SNR, antenna elements, and the number of snapshots. Simulations are conducted for the cases of three and two sources. Both coherent and noncoherent are considered for direction estimation with a single snapshot as well as multiple snapshots varying from 2 to 100 and SNR varying from 0 dB to 40 dB. The ULA consists of 25 antenna elements ($N = 12$). Additive white Gaussian noise (AWGN) is considered for generating the data signals received at the ULA. The simulations are run for 100 iterations for each value of the simulation parameter that is varied. Results of MATLAB simulations are shown in Fig. 4 through Fig. 9, which include RMSE vs SNR graphs, a histogram, an RMSE vs Snapshots graph, and RMSE vs Antenna Elements graphs. The performance of the proposed method is compared with that of URM.

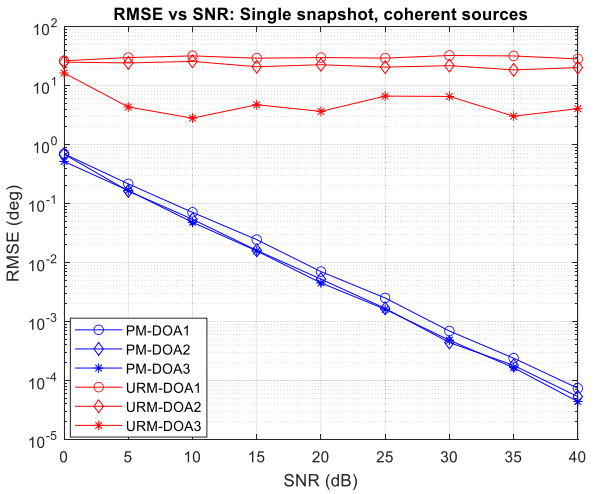

FIGURE 4. RMSE vs SNR: DOA estimation of three coherent sources with a single snapshot.

Fig. 4 shows the RMSE values plotted against SNR for the case of a single snapshot ($L = 1$) for three coherent sources. The blue curves are for the proposed method and red for URM. It is clear from the graph that URM fails to estimate the DOAs while the performance of the proposed method is impressive. Its performance improves with increasing SNR values while that of URM is unaffected. The single snapshot performance for noncoherent sources is very similar to that of coherent sources depicted in Fig. 4.

Fig. 5 and Fig. 6 show the RMSE values plotted against SNR for the case of 100 snapshots ($L = 100$) for coherent and noncoherent sources, respectively.

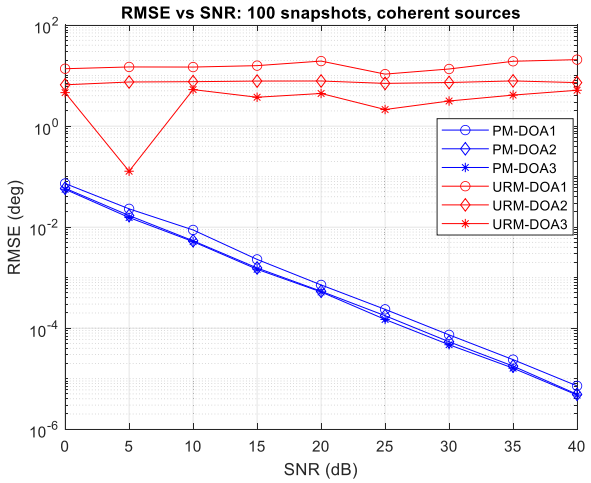

FIGURE 5. RMSE vs SNR: DOA estimation of three coherent sources with 100 snapshots.

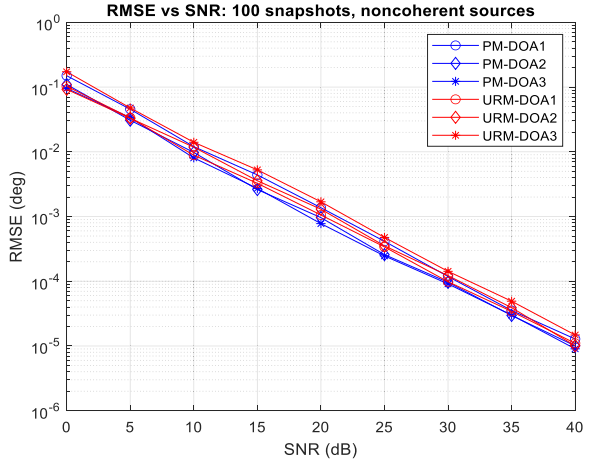

FIGURE 6. RMSE vs SNR: DOA estimation of three noncoherent sources with 100 snapshots.

It is clear from Fig. 5 that even for multiple snapshots, URM fails to estimate the DOAs for coherent sources at all SNR values while the proposed method demonstrates higher estimation accuracy compared with the single snapshot case. Its performance improves with increasing SNR values.

The graph in Fig. 6 below is for the DOA estimation of noncoherent sources with multiple snapshots where URM shows good performance in contrast with its performance for coherent sources. In this case, the performance of URM is on par with the proposed method.

The histogram chart in Fig. 7 below shows the estimation accuracy of the proposed method for three coherent sources located at 40°, 60°, and 80° from the ULA. DOA estimates are computed using only a single snapshot, 25 antenna elements, and SNR is 20 dB.

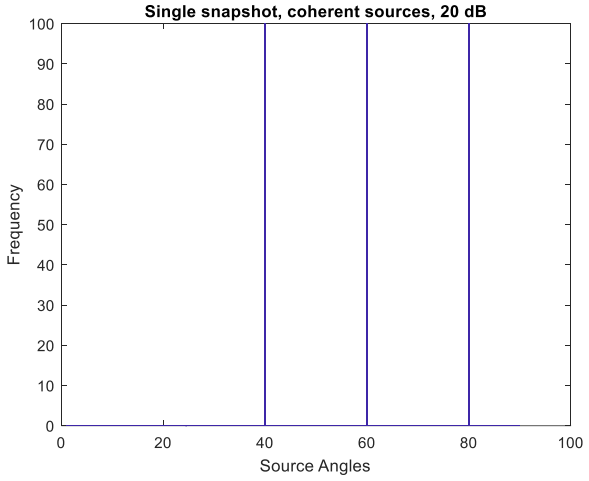

FIGURE 7. Histogram of DOA estimates of the proposed method for three coherent sources lying at 40°, 60° and 80° from the ULA.

The plots in Fig. 4 through Fig. 7 clearly demonstrate the superior performance of the proposed method for a single snapshot as well as multiple snapshots. While URM fails to estimate the DOAs of coherent sources for any number of snapshots, it accurately estimates the DOAs of noncoherent sources.

Simulations were also carried out for the case of two coherent sources to determine if URM shows better performance and estimates the DOAs correctly for a smaller number of sources. Fig. 8 below shows the DOA estimation performance for two coherent sources with a single snapshot. URM again fails to estimate the DOAs correctly while the proposed method shows high accuracy.

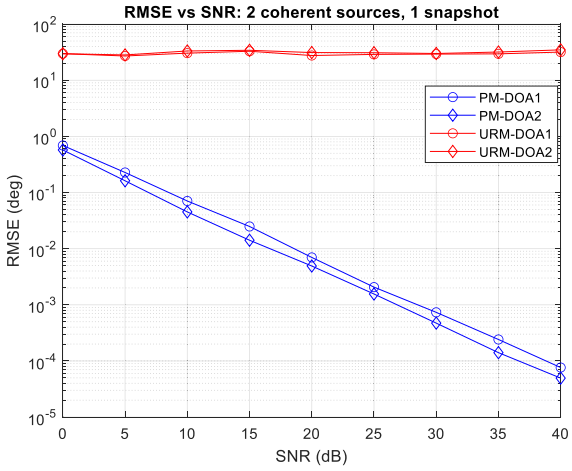

FIGURE 8. RMSE vs SNR: DOA estimation of two coherent sources with a single snapshot.

Next, the DOA estimation performance for URM was evaluated in the case of multiple snapshots. Fig. 9 shows the RMSE vs SNR graph for DOA estimation of two coherent sources with 100 snapshots. URM shows significantly

improved performance almost on par with the proposed method. This leads us to conclude that URM can accurately estimate up to two coherent sources with multiple snapshots but fails when only a single snapshot is used just as it did for the case of three coherent sources.

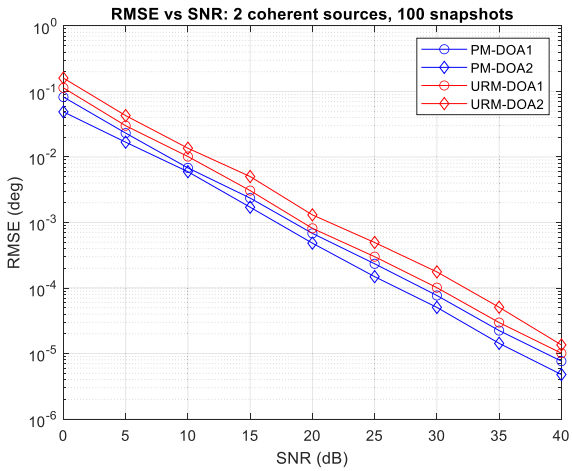

FIGURE 9. RMSE vs SNR: DOA estimation of two coherent sources with 100 snapshots.

The next graph in Fig. 10 shows the DOA estimation performance of the proposed method and URM for coherent sources with varying number of snapshots at 20 dB with 25 antenna elements. Snapshots are varied from 1 to 100 in steps of 8. The proposed method demonstrates consistent performance with high estimation accuracy while the RMSE values for URM hover around 10 degrees indicating high error in DOA estimation for coherent sources.

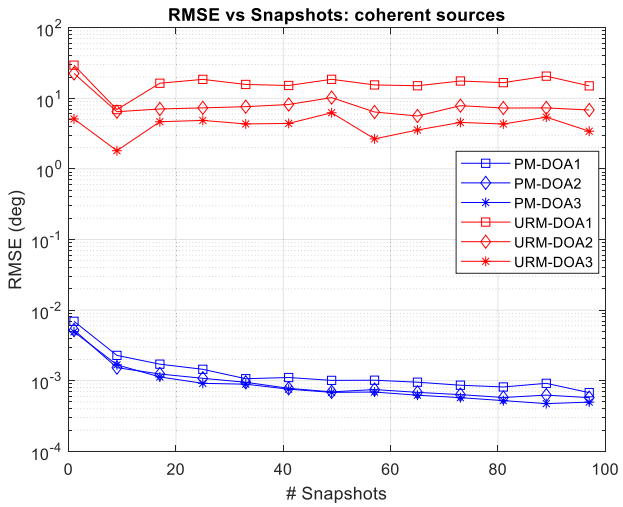

FIGURE 10. RMSE vs Snapshots: DOA estimation of three coherent sources with 25 antenna elements and 20 dB SNR.

Fig. 11 shows the DOA estimation performance for non-coherent sources with varying number of snapshots. While URM fails to estimate correctly with a single snapshot, it accurately estimates the DOAs with multiple snapshots with its performance matching that of the proposed method.

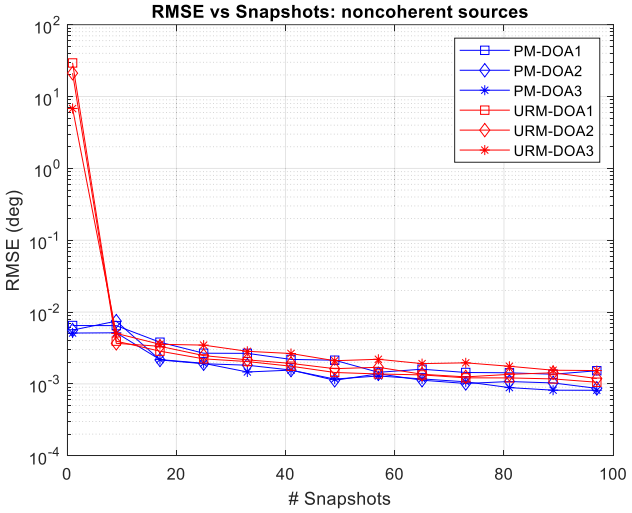

FIGURE 11. RMSE vs Snapshots: DOA estimation of three noncoherent sources with 25 antenna elements and 20 dB SNR.

DOA estimates were also computed for varying antenna elements. Fig. 12 below shows the RMSE values plotted against varying antenna elements for DOA estimation of coherent sources at 20 dB with a single snapshot. The three coherent sources were located at 40°, 60°, and 80° from the ULA. The graph in Fig. 12 (and Fig. 13) shows the number of antenna elements on the X-axis which are varied from 11 to 201 in steps of 10. While the proposed method demonstrates high estimation accuracy with its performance improving with increasing antenna elements, the URM suffers from high estimation error with no effect of increasing antenna elements.

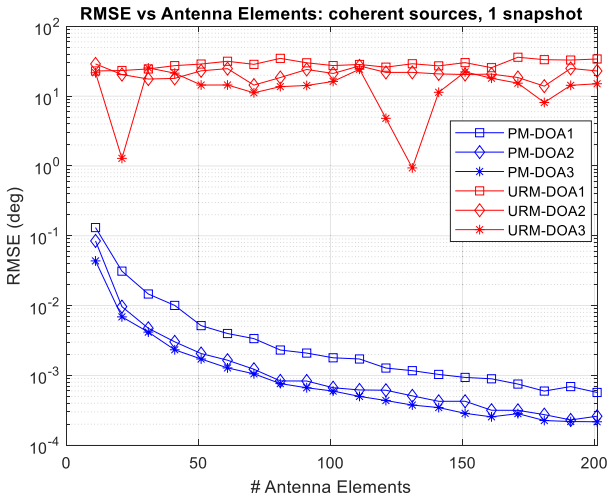

FIGURE 12. RMSE vs Antenna Elements: DOA estimation of three coherent sources with only 1 snapshot.

It also worth mentioning here that the performance of both methods for noncoherent sources using a single snapshot

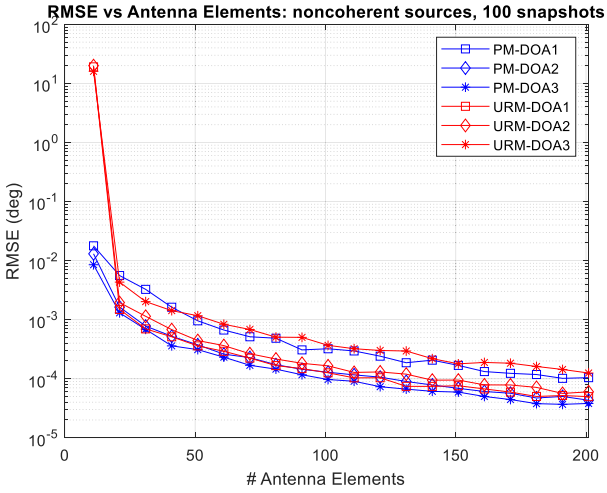

FIGURE 13. RMSE vs Antenna Elements: DOA estimation of three noncoherent sources with 100 snapshots.

is very similar to the case of coherent sources depicted in Fig. 12. However, the performance of URM for noncoherent sources for multiple snapshots is on par with the proposed method as depicted in Fig. 13 below.

The plots presented above provide strong evidence that the proposed method provides accurate DOA estimates for both coherent and non-coherent sources, even in scenarios with low signal-to-noise ratios (SNR), all achieved with just a single snapshot for computing the estimates.

Lastly, we assess the performance of the proposed method in terms of computation speed by examining the time required to compute the DOA estimates with respect to varying number of antenna elements in the ULA. We determined the computation times for both the proposed method and the URM method for DOA estimation involving three noncoherent sources with 100 snapshots, using MATLAB. The computation times are calculated over 100 iterations for each set of antenna elements in the ULA. Fig. 14 below illustrates the graph depicting Computation Time vs. Antenna Elements, providing clear evidence that the proposed method is significantly faster in computing DOA estimates and the contrast in computation time with URM becomes increasingly evident as the number of antenna elements grows.

V. PROTOTYPE USRP SDR TESTBED

The validity of the proposed method has been confirmed through experimental testing conducted on a prototype setup constructed using the USRP-2901 [61], which is a software-defined radio platform developed by National Instruments (NI). This section outlines the configuration of the testbed, with Fig. 15 illustrating the prototype testbed that includes three transmitting antennas in the foreground and a 9-element uniform linear array of receiving antenna elements, as depicted in Fig. 16. The receiver block diagram depicting the internal modules of the USRP is shown in Fig. 17.

This testbed has been built using six (6) units of USRP-2901 and one (1) unit of Octoclock CDA-2990 as shown in Fig. 18. The USRP-2901 is used for signal acquisition and it consists of two channels (0 and 1) with two ports each for signal reception/transmission, as shown on the front panel of the device in Fig. 19. The CDA-2990 [62] is a multi-clock signal generator and is used for generating the timing signals required for the time synchronization of the signals received at the ULA, as shown in Fig. 20.

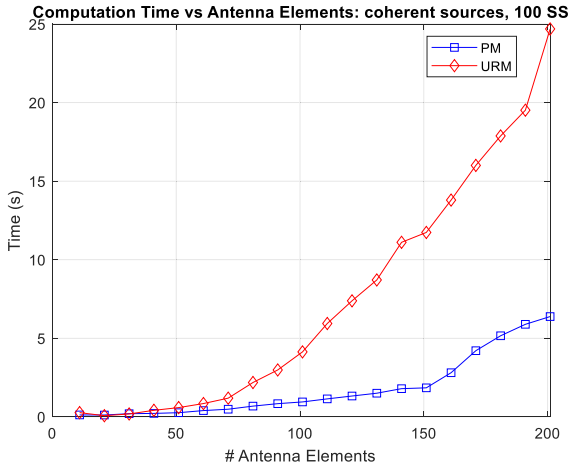

FIGURE 14. Computation Time vs Antenna Elements: DOA estimation of three noncoherent sources with 100 snapshots.

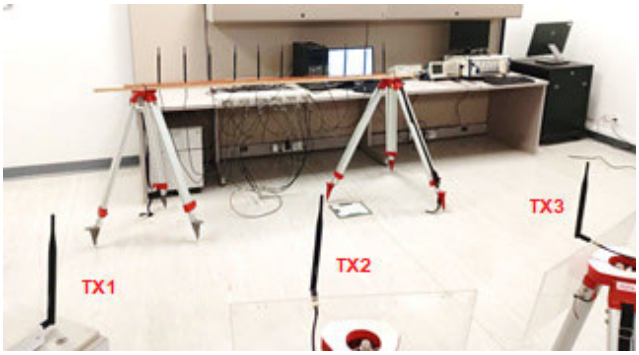

FIGURE 15. Prototype testbed consisting of a 9-element ULA for DOA estimation of up to 3 sources.

FIGURE 16. The 9-element ULA in the testbed.

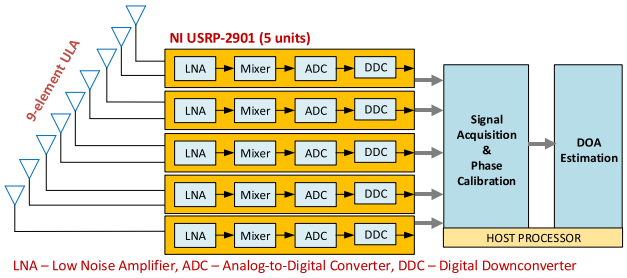

FIGURE 17. Receiver block diagram for the 9-element ULA.

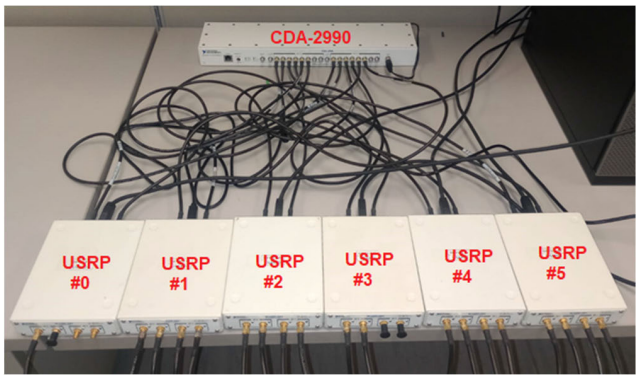

FIGURE 18. Prototype testbed built using six USRP-2901s and one CDA-2990.

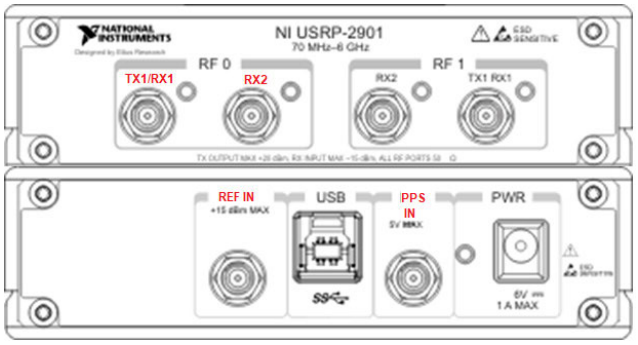

FIGURE 19. USRP-2901 front panel (top) and back panel (bottom).

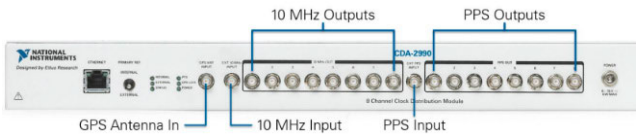

FIGURE 20. CDA-2990 front panel showing ports for PPS and REF IN.

The back panel of the USRP-2901 has ports for connecting a REF IN and PPS signals for timing synchronization. These signals are sourced from the CDA-2990 for each USRP unit. The CDA-2990 can support up to eight USRPs.

Fig. 21 illustrates the hardware connections within the receiver testbed designed for a 9-element ULA. This testbed is composed of five USRP-2901 Software-Defined Radio (SDR) units, and signal processing is managed by a host PC. The ULA, consisting of nine antennas, is linked to nine out of the ten available TX1/RX1 channels distributed across the five USRP-2901 units. An additional sixth USRP-2901 unit is employed for generating the reference signal for phase synchronization. This signal is input into RX2 ports of the remaining five USRP-2901 units. All USRPs establish connections with the host PC via USB ports.

A. PHASE SYNCHRONIZATION OF RX CHANNELS

Before acquiring the target data signals required for DOA estimates based on the phase delay between receiving channels, it is imperative to carry out both time and phase synchronization for each USRP device. Time synchronization is established through the use of the CDA-2990 module, a high-precision 8-channel timing reference system. To achieve this synchronization, a 10 MHz REF signal (indicated by the cyan-colored line) and a PPS (Pulse Per Second) signal (represented by the maroon-colored line), both from the CDA-2990, are connected to the REF IN and PPS inputs on each USRP-2901 unit, ensuring synchronization across this 9-channel system. It's noteworthy that a single CDA-2990 unit can support up to 8 USRP-2901 units.

Attaining phase synchronization is a vital but complex task when working with USRPs. These devices lack a shared local oscillator (LO), resulting in gradual phase drift over time. As a result, it becomes necessary to conduct phase calibration before each instance of data signal acquisition for further processing. It is important to note that phase synchronization can only commence after successful time synchronization of the USRPs has been achieved. The phase synchronization and signal acquisition procedures are illustrated in Fig. 22 below.

In the receiver part of the testbed depicted in Fig. 18, the task of achieving phase synchronization is accomplished using a single USRP-2901 unit, denoted as USRP #0. This unit is employed to generate a 10 kHz reference signal, which is subsequently up-converted to 1 GHz. As illustrated in Fig. 21 and Fig. 22, this reference signal (indicated by the green-colored line) is supplied to the RX2 channels on the remaining USRPs, numbered from 1 to 5 in Fig. 18. To execute this synchronization, a LabVIEW [63] graphical program has been developed that reads the reference signal and calculates the phase offset between the reference channel (channel 0) and each of the adjacent receive channels on both sides of the reference channel. This phase offset is then added to the data signals received from the 9-channel ULA (antennas connected to the TX/RX ports on the USRPs) to achieve phase synchronization. The phase synchronization and signal acquisition process is shown in Fig. 22 while the real-time phase synchronized signals are depicted in Fig. 23. The two sets of signals observed in Fig. 23 are the synchronized signals on either side of the reference channel.

After phase synchronization of the receive channels, the system is now ready to acquire the source signals from the ULA and compute the DOA estimates of the incident source signals.

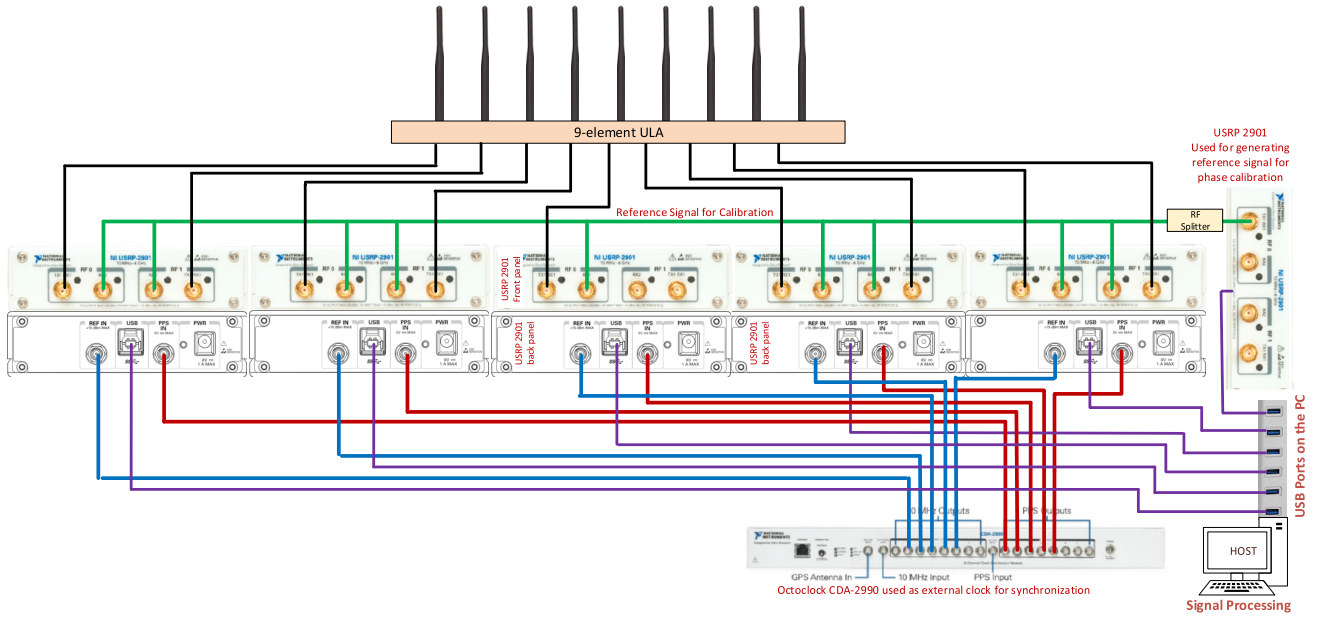

FIGURE 21. Detailed connection diagram of the 9-element ULA receiver testbed.

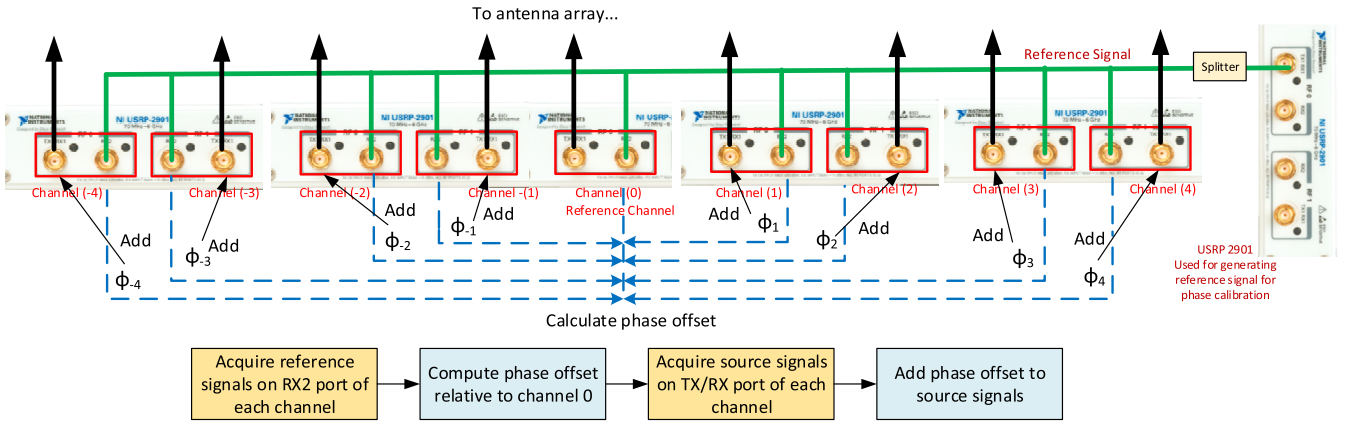

FIGURE 22. Phase Synchronization of five USRP-2901s using a reference signal generated by another USRP-2901.

VI. REAL-TIME DOA ESTIMATION

The proposed algorithm has been experimentally validated on the prototype testbed shown in Fig. 15. Three coherent sources were placed at arbitrary locations in the far-field region of the ULA. One USRP-2901 unit was used as a transmitter and connected to three omni-directional antennas using an RF splitter. The frequency of the signal was chosen as 1 GHz and the antenna elements on the receiving ULA were placed 15 cm apart corresponding to half the wavelength of the signal. The proposed algorithm was implemented using linear algebra and signal processing modules available in LabVIEW. DOA estimates were computed using only a single snapshot on the host PC. SNR of the source signals was varied from 5 dB to 40 dB in steps of 5 dB and 100 iterations were performed for each SNR value.

In Fig. 25, a screenshot of the user interface (UI) is shown for the real-time direction of arrival (DOA) estimation program developed in LabVIEW. The top left chart displays the received reference signals in real-time, before phase synchronization, while the bottom left chart depicts the signals after synchronization has been performed. On the top right, synchronized target (source) signals are shown. Finally, in the bottom right corner, the real-time DOA estimates computed for both the proposed method and URM are displayed.

After phase synchronization of all RX channels with respect to the reference channel, data signals acquired from the ULA are processed by the host PC and DOA estimates are computed for the proposed method and URM. Fig. 24 below shows the location of three source signals placed at 20^o, 65^o, and 110^o from the 9-element ULA.

One USRP-2901 unit is used as a transmitter and three transmit antennae connected to the TX/RX port of the USRP using a 4-way RF splitter are used to generate the three

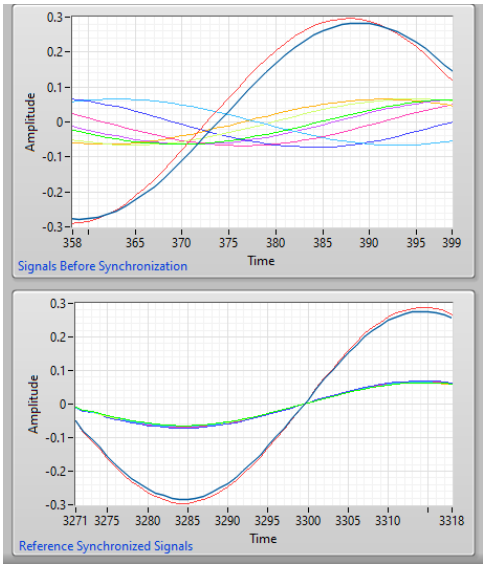

FIGURE 23. Reference signals before and after phase synchronization.

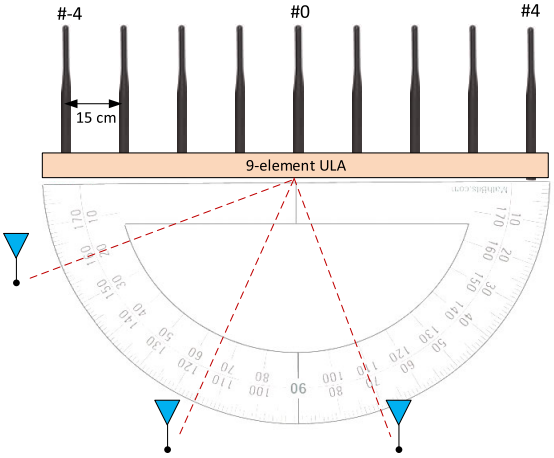

FIGURE 24. Three RF signals located at 20°, 65°, and 110° from the ULA.

coherent signals (freq.: 1 GHz, gain: 20 dB). The data signals received at the ULA are used for computing the real-time DOA estimates by the proposed algorithm as well as unitary root-MUSIC (URM). Fig. 26 shows one instance of the real-time DOA estimates computed for the three source signals for the proposed method and URM.

Fig. 27 displays a chart depicting the root mean square error (RMSE) in relation to SNR for DOA estimates derived from real-time experiments carried out on the prototype testbed. These experiments calculate the DOA estimates for both the proposed method and the URM method, and they involve three coherent signals positioned at 20^o, 65^o, and 110^o, respectively, relative to the ULA. The SNR values are represented on the horizontal axis, ranging from 0 dB to 35 dB. For each SNR value, RMSE values are computed for every DOA estimate, considering 100 successful trials, with

TABLE 3. Mean DOA estimates from real-time experiments for DOA estimation of three sources at 20 dB.

Source Locations			Proposed Method		
SRC1	SRC2	SRC3	SRC1	SRC2	SRC3
25	50	85	25.76	50.85	85.52
40	60	80	41.14	60.61	80.56
20	65	110	20.78	66.04	109.14
30	70	100	30.42	70.66	100.85
50	80	120	51.11	80.53	121.25

one snapshot taken in each trial. The chart shows average RMSE values for all sources together on a logarithmic scale.

Table 3 shows real-time DOA estimates on the host processor for three sources placed at arbitrary locations from the ULA reference. The source signals are transmitted at SNR of 20 dB. The table displays mean DOA values for the proposed method from 100 iterations with 1 snapshot in each iteration. DOA estimates for URM are not shown in the table due to the fact that all estimates deviate from the true values by around ± 9 to ± 18 degrees

It is clear from Fig. 26, Fig. 27, and Table 3 that the proposed method works well even with a single snapshot and it has higher estimation accuracy since the DOA estimates for the proposed method are closer to the actual locations of the three source signals compared with those of URM. It works well even at low SNR values.

The performance of the proposed method has been successfully validated experimentally in real-time using the 9-element ULA. However, the real-time estimation accuracy can be improved with a bigger ULA consisting of more antenna elements. Limited hardware resources allowed for only a 9-element ULA to be deployed on the prototype testbed.

VII. CONCLUSION

This paper presents a novel DOA estimation method that can accurately estimate the angles of arrival of multiple narrowband RF signals using only a single snapshot. It can accurately estimate both coherent and noncoherent signals. The proposed method offers several advantages over existing methods such as the unitary root-MUSIC. It has high estimation accuracy and low computation cost. It uses a Toeplitz structure data matrix and does not require the computation of a covariance matrix. The proposed method also employs a novel method for converting a complex-valued matrix to a real-valued matrix without the need for unitary transformations. Use of real-valued matrices reduces computation cost by a factor of 4 when compared with processing complex-valued matrices. The proposed method reduces the complexity further by employing QR decomposition method for extracting the signal and noise subspaces instead of the computationally expensive EVD or SVD. Another advantage

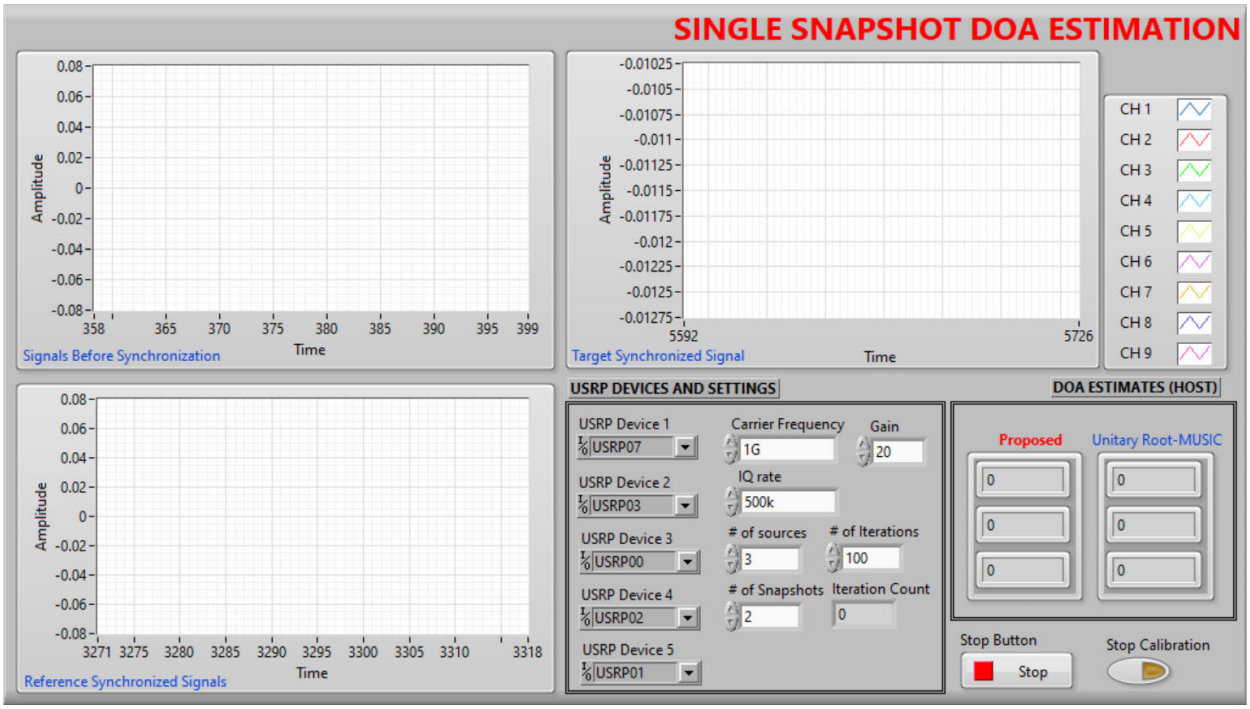

FIGURE 25. Graphical User Interface (GUI) of the LabVIEW program developed for real-time DOA estimation using a single snapshot.

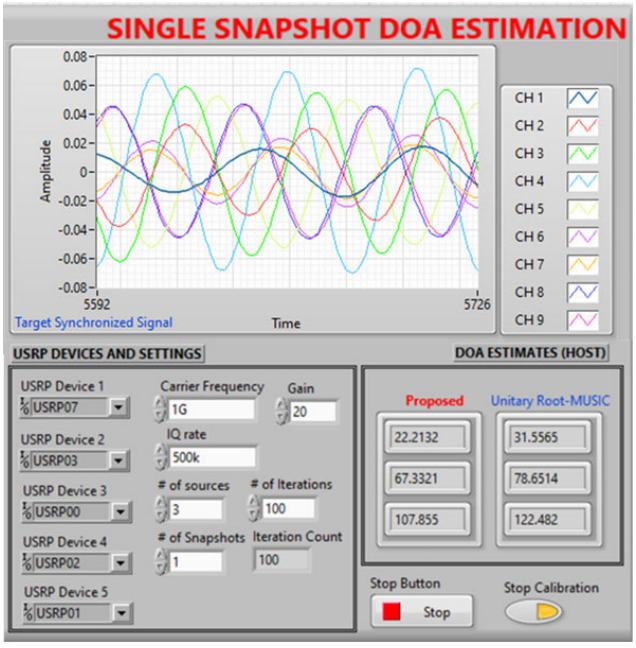

FIGURE 26. Screenshot - Real-time estimates for three source signals located at 20°, 65°, and 110° from the 9-element ULA.

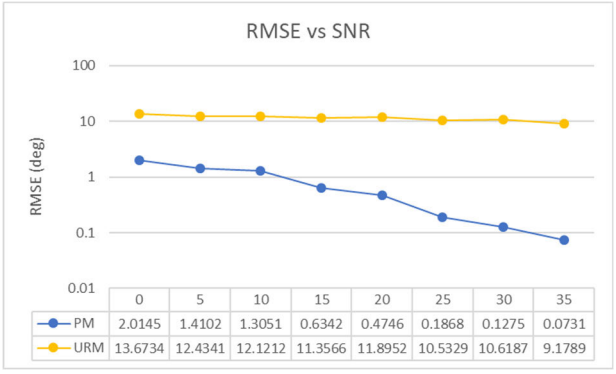

FIGURE 27. RMSE vs SNR for DOA estimation of three source signals located at 20°, 65°, and 110° from the 9-element ULA.

of QR over EVD/SVD is that it avoids real-valued matrices from reverting to complex-valued matrices which happens due to complex eigenvalues yielding complex eigenvectors. The proposed method was validated for estimation accuracy through both MATLAB simulations and real-time experiments. Its performance was benchmarked against unitary root-MUSIC and found to be superior.

DOA estimation using a single snapshot, the use of real-valued matrices and QR decomposition for extracting the signal and noise subspaces results in significantly reduced computational complexity for the proposed method allowing for faster estimation and fewer resources consumption while providing very high estimation accuracy. These advantages of the proposed method render it highly suitable for deployment in massive MIMO systems, advanced wireless communications networks, and related practical applications.

REFERENCES

[1] R. T. Compton Jr., *Adaptive Array—Concepts and Performance*. Englewood Cliffs, NJ, USA: Prentice-Hall, 1988.

[2] R. A. Monzingo and T. W. Miller, *Introduction to Adaptive Arrays*. New York, NY, USA: Wiley, 1980.

[3] J. E. Hudson, *Adaptive Array Principles*. London, U.K.: Peter Peregrinus, 1981.

[4] J. C. Liberti and T. S. Rappaport Jr., *Smart Antennas for Wireless Communications*. Upper Saddle River, NJ, USA: Prentice-Hall, 1999.

[5] A. Paulraj, R. Roy, and T. Kailath, "Estimation of signal parameters via rotational invariance techniques—ESPRIT," in *Proc. 19th Asilomar Conf. Circuits, Syst. Comput.,*, 1985, pp. 83–89.

[6] P. Yang, F. Yang, and Z.-P. Nie, "DOA estimation with sub-array divided technique and interporlated ESPRIT algorithm on a cylindrical conformal array antenna," *Prog. Electromagn. Res.*, vol. 103, pp. 201–216, 2010.

[7] Y.-S. Kim and Y.-S. Kim, "Improved resolution capability via virtual expansion of array," *Electron. Lett.*, vol. 35, no. 19, p. 1596, 1999.

[8] G. H. Golub and C. F. Van Loan, *Matrix Computations*, 3rd ed. Baltimore, MD, USA: John Hopkins Univ. Press, 1996.

[9] C. A. Balanis and P. I. Ioannides, *Introduction to Smart Antennas*. San Rafael, CA, USA: Morgan & Claypool, 2007.

[10] Y. Yang, C. Wan, C. Sun, and Q. Wang, "DOA estimation for coherent sources in beamspace using spatial smoothing," in *Proc. 4th Int. Conf. Inf., Commun. Signal Process., 4th Pacific Rim Conf. Multimedia*, vol. 2, 2003, pp. 1028–1032.

[11] Q. Chen and R. Liu, "On the explanation of spatial smoothing in MUSIC algorithm for coherent sources," in *Proc. Int. Conf. Inf. Sci. Technol.*, Mar. 2011, pp. 699–702.

[12] S. Changgan and L. Yumin, "An improved forward/backward spatial smoothing root-MUSIC algorithm based on signal decorrelation," in *Proc. IEEE Workshop Adv. Res. Technol. Ind. Appl. (WARTIA)*, Sep. 2014, pp. 1252–1255.

[13] G.-T. Pham, P. Loubaton, and P. Vallet, "Performance analysis of spatial smoothing schemes in the context of large arrays," *IEEE Trans. Signal Process.*, vol. 64, no. 1, pp. 160–172, Jan. 2016.

[14] Z. Zhang, F. Wen, J. Shi, J. He, and T.-K. Truong, "2D-DOA estimation for coherent signals via a polarized uniform rectangular array," *IEEE Signal Process. Lett.*, vol. 30, pp. 893–897, 2023, doi: 10.1109/LSP.2023.3296038.

[15] A. A. Hussain, N. Tayem, A.-H. Soliman, and R. M. Radaydeh, "Novel forward/backward signal space for DOA estimation of coherent RF signals," in *Proc. 14th Int. Conf. Signal Process. Syst. (ICSPS)*, Jiangsu, China, Nov. 2022.

[16] A. A. Hussain, N. Tayem, and A.-H. Soliman, "Computationally efficient forward/backward averaged DOA estimation of coherent sources in pairs," in *Proc. IEEE 94th Veh. Technol. Conf. (VTC-Fall)*, Sep. 2021, pp. 1–7.

[17] X.-Q. Hu, J.-W. Chen, H. Chen, and Y.-L. Wang, "Estimation DOAs of the coherent sources based on Toeplitz decorrelation," in *Proc. Congr. Image Signal Process.*, vol. 5, May 2008, pp. 54–58.

[18] X. Zhang, X. Liu, and H. Yu, "Improved MUSIC algorithm for DOA estimation of coherent signals via Toeplitz and fourth-order-cumulants," *Int. J. Control Autom.*, vol. 8, no. 10, pp. 261–272, Oct. 2015.

[19] A. Goian, M. I. AlHajri, R. M. Shubair, L. Weruaga, A. R. Kulaib, R. AlMemari, and M. Darweesh, "Fast detection of coherent signals using pre-conditioned root-MUSIC based on Toeplitz matrix reconstruction," in *Proc. IEEE 11th Int. Conf. Wireless Mobile Comput., Netw. Commun. (WiMob)*, Oct. 2015, pp. 168–174.

[20] J. Bai, X. Shen, H. Wang, and Y. Liu, "Improved Toeplitz algorithms to coherent sources DOA estimation," in *Proc. Int. Conf. Measuring Technol. Mechatronics Autom.*, vol. 2, Mar. 2010, pp. 442–445.

[21] Z.-M. Liu, L. Wu, and P. S. Yu, "Deep learning techniques for direction of arrival estimation," in *Applications of Deep Learning in Electromagnetics: Teaching Maxwell's Equations to Machines*, vol. 231. Rijeka, Croatia: SciTech, 2023.

[22] G. K. Papageorgiou, M. Sellathurai, and Y. C. Eldar, "Deep networks for direction-of-arrival estimation in low SNR," *IEEE Trans. Signal Process.*, vol. 69, pp. 3714–3729, 2021.

[23] J. Fuchs, M. Gardill, M. Lübke, A. Dubey, and F. Lurz, "A machine learning perspective on automotive radar direction of arrival estimation," *IEEE Access*, vol. 10, pp. 6775–6797, 2022.

[24] M. Yang, B. Ai, R. He, H. Chen, Z. Ma, and Z. Zhong, "Angle-of-arrival estimation for vehicle-to-vehicle communications based on machine learning," in *Proc. Int. Conf. Wireless Commun. Signal Process. (WCSP)*, Nanjing, China, Oct. 2020, pp. 154–158.

[25] M. Yang, B. Ai, R. He, C. Huang, Z. Ma, Z. Zhong, J. Wang, L. Pei, Y. Li, and J. Li, "Machine-learning-based fast angle-of-arrival recognition for vehicular communications," *IEEE Trans. Veh. Technol.*, vol. 70, no. 2, pp. 1592–1605, Feb. 2021.

[26] A. Alhamed, N. Tayem, T. Alshawi, S. Alshebeili, A. Alsuwailem, and A. Hussain, "FPGA-based real-time implementation for direction-of-arrival estimation," *J. Eng.*, vol. 2017, no. 6, pp. 260–265, Jun. 2017, doi: 10.1049/joe.2017.0165.

[27] A. A. Hussain, N. Tayem, M. O. Butt, A.-H. Soliman, A. Alhamed, and S. Alshebeili, "FPGA hardware implementation of DOA estimation algorithm employing LU decomposition," *IEEE Access*, vol. 6, pp. 17666–17680, 2018, doi: 10.1109/ACCESS.2018.2820122.

[28] A. A. Hussain, N. Tayem, and A.-H. Soliman, "LDL decomposition-based FGPA real-time implementation of DOA estimation," in *Proc. 52nd Asilomar Conf. Signals, Syst., Comput.*, Pacific Grove, CA, USA, Oct. 2018, pp. 1163–1168, doi: 10.1109/ACSSC.2018.8645387.

[29] S. O. Al-Jazzar, "Angle of arrival estimation using Cholesky decomposition," *Int. J. Antennas Propag.*, vol. 2012, Jun. 2012, Art. no. 803617.

[30] A. A. Hussain, N. Tayem, and A.-H. Soliman, "Matrix decomposition methods for efficient hardware implementation of DOA estimation algorithms: A performance comparison," in *Proc. 4th Int. Conf. Workshops Recent Adv. Innov. Eng. (ICRAIE)*, Penang, Malaysia, Nov. 2019.

[31] M. Muhammad, M. Li, Q. Abbasi, C. Goh, and M. A. Imran, "A covariance matrix reconstruction approach for single snapshot direction of arrival estimation," *Sensors*, vol. 22, no. 8, p. 3096, Apr. 2022, doi: 10.3390/s22083096.

[32] R. Wu, M. Wang, and Z. Zhang, "Computationally efficient DOA and carrier estimation for coherent signal using single snapshot and its time-delay replications," *IEEE Trans. Aerosp. Electron. Syst.*, vol. 57, no. 4, pp. 2469–2480, Aug. 2021, doi: 10.1109/TAES.2021.3061821.

[33] R. T. O'Brien and K. Kiriakidis, "Single-snapshot robust direction finding," *IEEE Trans. Signal Process.*, vol. 53, no. 6, pp. 1964–1978, Jun. 2005.

[34] A. S. Assoa, A. Bhat, S. Ryu, and A. Raychowdhury, "A scalable platform for single-snapshot direction of arrival (DOA) estimation in massive MIMO systems," in *Proc. Great Lakes Symp. VLSI*, New York, NY, USA, Jun. 2023, pp. 631–637, doi: 10.1145/3583781.3590212.

[35] A. G. Raj and J. H. McClellan, "Single snapshot super-resolution DOA estimation for arbitrary array geometries," *IEEE Signal Process. Lett.*, vol. 26, no. 1, pp. 119–123, Jan. 2019, doi: 10.1109/LSP.2018.2881927.

[36] H. A. Tanti, A. Datta, and S. Ananthakrishnan, "Snapshot averaged matrix pencil method (SAM) for direction of arrival estimation," *Exp. Astron.*, vol. 56, no. 1, pp. 267–292, Aug. 2023, doi: 10.1007/s10686-023-09897-6.

[37] S. Mazokha, S. Naderi, G. I. Orfanidis, G. Sklivanitis, D. A. Pados, and J. O. Hallstrom, "Single-sample direction-of-arrival estimation for fast and robust 3D localization with real measurements from a massive MIMO system," in *Proc. IEEE Int. Conf. Acoust., Speech Signal Process. (ICASSP)*, Rhodes Island, Greece, Jun. 2023, pp. 1–5, doi: 10.1109/ICASSP49357.2023.10096647.

[38] R. Cao, B. Liu, F. Gao, and X. Zhang, "A low-complex one-snapshot DOA estimation algorithm with massive ULA," *IEEE Commun. Lett.*, vol. 21, no. 5, pp. 1071–1074, May 2017.

[39] Q. Wang, Z. Zhao, and Z. Chen, "Fast compressive sensing DOA estimation via ADMM solver," in *Proc. IEEE Int. Conf. Inf. Autom. (ICIA)*, Jul. 2017, pp. 53–57.

[40] N. Dong, L. Zhang, H. Zhou, X. Li, S. Wu, and X. Liu, "Two-stage fast matching pursuit algorithm for multi-target localization," *IEEE Access*, vol. 11, pp. 66318–66326, 2023, doi: 10.1109/ACCESS.2023.3290031.

[41] R. K. Arumugam, A. Froehly, R. Herschel, P. Wallrath, and N. Pohl, "Direction of arrival estimation on sparse arrays using compressive sensing and MUSIC," in *Proc. 17th Eur. Conf. Antennas Propag. (EuCAP)*, Florence, Italy, Mar. 2023, pp. 1–5, doi: 10.23919/EuCAP57121.2023.10133647.

[42] J. R. Mohammed, "High-resolution direction of arrival estimation method based on sparse arrays with minimum number of elements," *J. Telecommun. Inf. Technol.*, vol. 1, no. 2021, pp. 8–14, Mar. 2021, doi: 10.26636/jtit.2021.143720.
[43] A. Das, W. S. Hodgkiss, and P. Gerstoft, "Coherent multipath direction-of-arrival resolution using compressed sensing," *IEEE J. Ocean. Eng.*, vol. 42, no. 2, pp. 494–505, Apr. 2017, doi: 10.1109/JOE.2016.2576198.
[44] K. Usman, H. Gunawan, and A. B. Suksmono, "Optimal thresholding for direction of arrival estimation using compressive sensing," in *Proc. Int. Conf. Control, Electron., Renew. Energy Commun. (ICCEREC)*, Bandung, Indonesia, Dec. 2018, pp. 115–121, doi: 10.1109/ICCEREC.2018.8712094.
[45] P. Zhao, G. Hu, Z. Qu, and L. Wang, "Enhanced nested array configuration with hole-free co-array and increasing degrees of freedom for DOA estimation," *IEEE Commun. Lett.*, vol. 23, no. 12, pp. 2224–2228, Dec. 2019, doi: 10.1109/LCOMM.2019.2947585.
[46] W. T. Li, Y. J. Lei, and X. W. Shi, "DOA estimation of time-modulated linear array based on sparse signal recovery," *IEEE Antennas Wireless Propag. Lett.*, vol. 16, pp. 2336–2340, 2017, doi: 10.1109/LAWP.2017.2717931.
[47] W. Xiaochuan, H. Bin, C. Qiushi, Z. Xin, Y. Qiang, and D. Weibo, "Grid evolution: An iterative reweighted algorithm for off-grid DOA estimation with gain/phase uncertainties," in *Proc. IEEE Int. Conf. Signal, Inf. Data Process. (ICSIDP)*, Chongqing, China, Dec. 2019, pp. 1–4, doi: 10.1109/ICSIDP47821.2019.9173409.
[48] Z. Huang, W. Wang, B. Zhang, and D. Wang, "Measurement matrix design based on compressed sensing for DOA estimation," in *Proc. 14th IEEE Int. Conf. Signal Process. (ICSP)*, Beijing, China, Aug. 2018, pp. 167–171, doi: 10.1109/ICSP.2018.8652336.
[49] N. Tayem, "Real time implementation for DOA estimation methods on NI-PXI platform," *Prog. In Electromagn. Res. B*, vol. 59, pp. 103–121, 2014.
[50] A. A. Hussain, N. Tayem, A.-H. Soliman, and R. M. Radaydeh, "FPGA-based hardware implementation of computationally efficient multi-source DOA estimation algorithms," *IEEE Access*, vol. 7, pp. 88845–88858, 2019.
[51] F. M. Unlersen, E. Yaldiz, and S. T. Imeci, "FPGA based fast Bartlett DoA estimator for ULA antenna using parallel computing," *Appl. Comput. Electromagn. Soc. J.*, vol. 33, no. 4, pp. 450–459, Apr. 2018.
[52] M. Devendra and K. Manjunathachari, "Direction of arrival estimation using MUSIC algorithm in FPGA: Hardware software co-design," *Int. J. Appl. Eng. Res.*, vol. 11, no. 5, pp. 3112–3116, 2016.
[53] J. Yan, Y. Huang, H. Xu, and G. A. E. Vandenbosch, "Hardware acceleration of MUSIC based DoA estimator in MUBTS," in *Proc. 8th Eur. Conf. Antennas Propag. (EuCAP)*, Apr. 2014, pp. 2561–2565.
[54] A. D. Redondo, T. Sanchez, C. Gomez, L. Betancur, and R. C. Hincapie, "MIMO SDR-based implementation of AoA algorithms for radio direction finding in spectrum sensing activities," in *Proc. IEEE Colombian Conf. Commun. Comput. (IEEE COLCOM)*, Colombia, May 2015, pp. 1–4.
[55] V. Goverdovsky, D. C. Yates, M. Willerton, C. Papavassiliou, and E. Yeatman, "Modular software-defined radio testbed for rapid prototyping of localization algorithms," *IEEE Trans. Instrum. Meas.*, vol. 65, no. 7, pp. 1577–1584, Jul. 2016.
[56] Z. Yang, L. Xie, and P. Stoica, "Vandermonde decomposition of multilevel Toeplitz matrices with application to multidimensional super-resolution," *IEEE Trans. Inf. Theory*, vol. 62, no. 6, pp. 3685–3701, Jun. 2016, doi: 10.1109/TIT.2016.2553041.
[57] C. Caratheodory and L. Fejer, "Uber den Zusammenhang der extremen von harmonischen funktionen mit ihren koeffizienten und über den picard-landau'schen satz," *Rendiconti del Circolo Matematico di Palermo*, vol. 32, no. 1, pp. 218–239, 1911.
[58] V. F. Pisarenko, "The retrieval of harmonics from a covariance function," *Geophys. J. Int.*, vol. 33, no. 3, pp. 347–366, Sep. 1973.
[59] D. M. Wilkes, S. D. Morgera, F. Noor, and M. H. Hayes, "A Hermitian Toeplitz matrix is unitarily similar to a real Toeplitz-plus-Hankel matrix," *IEEE Trans. Signal Process.*, vol. 39, no. 9, pp. 2146–2148, Sep. 1991, doi: 10.1109/78.134459.
[60] N. Tayem and M. Naraghi-Pour, "Unitary root MUSIC and unitary MUSIC with real-valued rank revealing triangular factorization," in *Proc. IEEE Mil. Commun. Conf. (MILCOM)*, Orlando, FL, USA, Oct. 2007, pp. 1–7, doi: 10.1109/MILCOM.2007.4454816.
[61] *USRP SDR 2901*. [Online]. Available: http://www.ni.com/en-lb/support/model.usrp-2901.html
[62] *Octo-clock CDA-2990 8-Channel Clock Distribution Module*. [Online]. Available: https://www.ettus.com/product/details/OctoClock-G
[63] *NI LabVIEW Software Platform*. [Online]. Available: http://www.ni.com/labview/

AHMED A. HUSSAIN received the M.S. degree in electrical and computer engineering from the University of Florida, Gainesville, FL, USA, in 1998. He was with Motorola as an Embedded Software Engineer. He is currently a Lecturer with the Department of Electrical Engineering, Prince Mohammad bin Fahd University. He has more than 20 years of university teaching experience in electrical engineering. His research interests include wireless communications, array signal processing, digital and embedded systems, and program assessment and accreditation. He has several research publications and U.S. patents in the above-mentioned areas of interest.

NIZAR TAYEM (Member, IEEE) received the Ph.D. degree in electrical engineering from Wichita State University, Wichita, KS, USA. He is currently an Assistant Professor with the Department of Electrical Engineering, Texas A&M University–Commerce, Commerce, TX, USA. He worked on research projects for Aerospace Sensor Networks Technology Thrust, Minority Leader's Program, and AFRL/Clarkson Aerospace. He is the author/coauthor of more than 60 research publications in recognized international journals and conferences. His research interests include signal processing algorithms for wireless communication systems, array signal processing, source localization, MIMO systems, channel estimation, and OFDM and OFDMA communication systems. He is a Senior Member of the Institute of Doctors Engineers and Scientists (IDES) and a regular reviewer of many well-known journals. He has served as the Editor-in-Chief for *International Journal on Electrical and Power Engineering* (ACEEE, USA).

ABDEL-HAMID SOLIMAN received the B.Sc. degree in electronic and telecommunications from the Arab Academy for Science, Technology and Maritime Transport, the M.Sc. degree in smart data acquisition systems from Alexandria University, and the Ph.D. degree in image/video processing from Staffordshire University. He is currently an Associate Professor in telecommunication and signal processing with the School of Digital, Technologies and Arts, Staffordshire University. He has a multi-disciplinary academic/research experience in digital signal processing, telecommunications, data acquisition systems, wireless sensor networks (WSN), and image/video processing. He is focusing on the research on harnessing these technologies to contribute to the smart cities applications. He has more than 27 years of working experience in higher education institutes. In addition to the research and teaching/learning activities, he is involved in several enterprise projects and consultancy activities for national and international companies. He is currently leading and involved in several European-funded projects in education, industry automation, and healthcare applications.